Geological framework for assessing variability in subsurface piping parameters underneath dikes in the Rhine-Meuse delta, the Netherlands

T.G. Winkels [*], K.M. Cohen, S.M. Knaake, H. Middelkoop, E. Stouthamer

Faculty of Geosciences, Department of Physical Geography, Utrecht University, the Netherlands

ABSTRACT

Dike failure due to piping – concentrated flow of seepage water underneath the dike during periods of high flood water levels – has been recognized as a major component of flood risk. Simulation models to predict piping in risk assessments require detailed information on subsurface characteristics such as sediment grain size and thickness of overburden layers. Quantitative local determination of these characteristics poses a major challenge in natural environments with a heterogeneous substrate. Geological knowledge on the natural genesis and resulting structure of the subsurface may provide useful information on the spatial variability of substrate characteristics. When correctly implemented, available subsurface geological information can provide for a-priori identification of dike sections of which the subsurface is susceptible to piping (strategic to new data collection), and a-posteriori screening of new collected field data (identifying unexpected values). In these two ways it has potential to reduce the uncertainty in parameter estimates for calculations that determine the potential occurrence of piping at a specific site. Here we describe a framework for using geological subsurface information for these assessments. Based on existing digital geological mapping products and knowledge of the geological development of the Rhine-Meuse delta, we first compiled a map that distinguishes primary hydrologically relevant units: upper main aquifer sands (*pre-deltaic subunits*), topped by the deltaic wedge aquitard that is dissected by channel belt sand bodies (*deltaic subunits*). We then used these spatial divisions in an analysis of digital borehole data (>130.000 locations, UU-LLG dataset), to provide quantitative information on grain sizes of the very top of sand bodies and non-sand overburden thicknesses, split per subunit and summarized for sub regions (lower delta, central delta, upper delta, delta rim sectors). This framework enables us to demonstrate to what extent the median grain size of the top of sand deposits varies within the delta. We quantitatively determined (1) a delta-scale longitudinal downstream fining trend due to drops in specific stream power through changes in gradient and substrate erodibility, (2) pulsed variations associated with local uptake and reworking of pre-deltaic sediments within channel belts. Although tailored for the Rhine-Meuse delta, utilizing geological knowledge as a substantiation for grouping of subsurface data underneath local dike sections can be transposed for such applications in delta regions elsewhere. This regionalization of the delta plain can greatly help streamline data acquisition, anticipating growing availability of medium to high density subsurface datasets in increasingly urbanized deltas with managed rivers around the world.

1. Introduction

Dikes form an essential part of the primary flood defences along the rivers Rhine and Meuse in the Netherlands. The four main branches of these rivers are flanked with approximately 2600 km of dikes. Current governmental procedural standards for dike design, maintenance and safety assessments are high. The current risk-based approach for flood protection considers multiple types of failure mechanisms of dikes, such as piping, macro-instability and overtopping (De Waal, 2018; MinIM, 2016). For the Rhine branches, discharges corresponding to an undivided 16,000–18,000 m^3/s at the delta apex (Lobith; Fig. 1A) feed typical assessments and are attributed recurrence times exceeding 1250 years. A discharge of12,600 m^3/s is the highest measured value in the past century and peaks reaching 8000 m^3/s occur at an average recurrence time of 5 years. Dike maintenance and flood safety assessments further consider the detailed dike geometry and subsurface build-up in evaluating the probabilities of the various dike failure mechanisms.

A prime failure mechanism threatening dike stability, in which the

---

subsurface plays a dominant role, is 'piping': the erosional formation of, usually small, pipes along preferential seepage pathways in sandy substrate situated immediately below dikes, during high discharge events. Susceptibility to piping is governed by local conditions of the natural substrate and the magnitude of potential triggers in the form of hydraulic pressure gradients driven by rising flood water levels (e.g. Kolb, 1975; Wolff, 2002; Apel et al., 2006; Glynn et al., 2012; Kanning, 2012). Clearly, the piping susceptibility increases where dike height and design flood levels are raised. In the Netherlands, piping is currently seen as the primary threat for dike destabilization under conditions of high peak discharge (VNK, 2015; Kruse and Hijma, 2015). As a threat to dike stability it is recognized worldwide (e.g. Di Baldassarre et al., 2010; Foster et al., 2000; Glynn et al., 2012; Bridle and Fell, 2013) and for that reason it has long been studied both at the process scale and for local cases (e.g. Bligh, 1910; Lane, 1934; Sellmeijer, 1988; Van Beek et al.,

2010; Glynn et al., 2012; Robbins and Van Beek, 2015; Martínez et al., 2016). In the Netherlands, assessment of piping susceptibility for predetermined dike segments is done through protocolised schematisations and calculations. This requires various input parameters on subsurface characteristics, including a measure of the grain-size distribution (D_{70}) and permeability (K_{sat}) of sand bodies and a value representing aquitard overburden thickness. The large natural variability within these subsurface characteristics, however, poses a challenge for setting up detailed subsurface parameterizations needed for piping calculations. This heterogeneity at grain to delta scale is due to geological processes, implying it should not be treated as something random. The range of scales over which heterogeneity stretches makes that it cannot simply be dealt with by just collecting more data. In fact: the more data has been collected, the more heterogeneous the subsurface turned out to be.

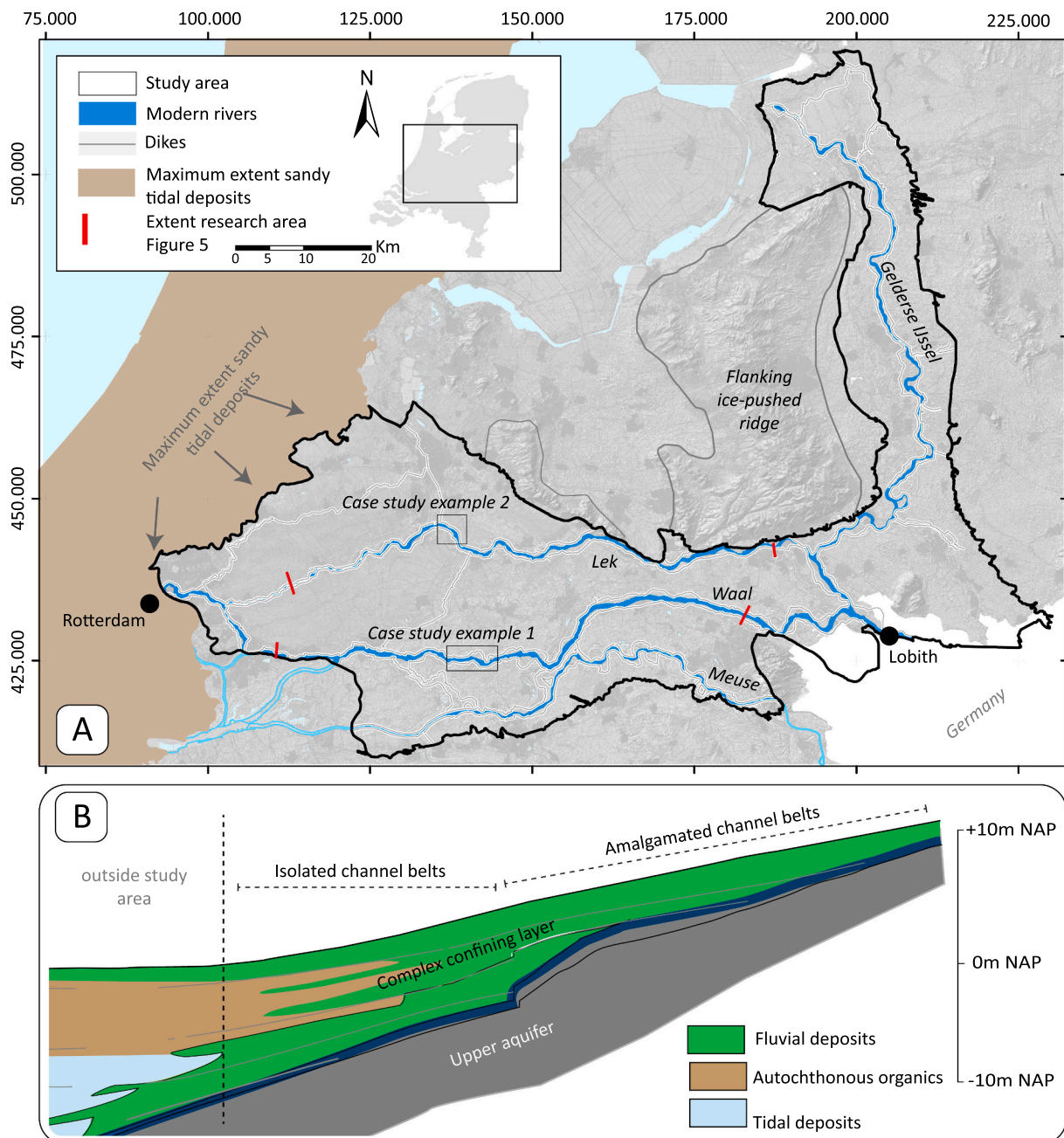Realizing that subsurface variation and heterogeneity carry

Fig. 1. Location (A) and cross section (B) of the study area: the fluvial dominated part of the Rhine-Meuse delta, including the present major rivers (active branches of Rhine and Meuse) and their embanked floodplains (bound by artificial levees: 'dikes').

uncertainty into geotechnical calculations, current Dutch governmental directives on dike safety assessments require stochastic approaches to parameterizing piping calculations and subsurface reconstructions (Kruse and Hijma, 2015). This includes considering multiple subsurface build-up scenarios to incorporate mapping uncertainty (e.g. Hijma and Lam, 2015 – their Table 3.1) and continues with specifying subsurface characteristics for each substrate unit. In practice, this means one needs to (i) define spatial divisions and (ii) pick representative values for D_{70} and K_{sat} and associated variance coefficients. To aid parameter choices for dike assessments in the Netherlands, the WTI-SOS system (Hijma and Lam, 2015) provides lists of default values, which on the basis of local data can be adapted to come to a final input values. Main scientific aims connected to this practice are (i) to assess and quantify spatial variability in subsurface characteristics using a geological spatial division framework, and (ii) to explore how knowledge on the geological context (past processes and their outcome) is suitably applied in the subsequent tuning of schematization and parameterization of local situations. Research effort along these lines may reveal what part of the variance is systematic (and mappable) and what remains random (or unmappable), besides giving insight allowing to improve data acquisition and how to combine and convert lithological information into the calculation parameters. In this paper we provide a geological framework– a geogenetic division scheme separating generations of deltaic sand bodies and pre-deltaic sands that constitute potential piping-susceptible substrates – allowing for capturing subsurface variability relevant to the piping process across the fluvial dominated part of the Rhine-Meuse delta (Fig. 1A). To underpin the division scheme, we first demonstrate the relevance of geologically subdividing the delta plain substrate underneath dikes for the parameterization of piping calculations, and describe the incorporated regional geological knowledge for the deltaic wedge (complex confining layer) and the palaeovalley substrate (first aquifer). We then present a map of the upper sand bodies that used the geogenetic division scheme, storing and showing geological framework of the shallow s sandy substrate through the delta (Fig. 4). The map is used to establish a dataset of quantified architectural and lithological properties of the mapped units and regional trends therein, derived from the extensive dataset of lithological core descriptions of the Holocene Rhine-Meuse delta (UU-LLG dataset; Cohen et al., 2017a).

We evaluate geological causation to explain regional trends and we discuss remaining local variability in subsurface characterizing parameters for piping calculations for the Rhine-Meuse delta and how to apply it in dike safety assessments. Lastly we reflect on the Dutch data situation that triggered the wish to incorporate regional default values and our geological framework approach, and whether this can be utilized in other areas of the world as well.

2. Piping and subsurface characteristics

In this section we describe the piping process and subsurface related characteristics that are used as parameters in piping assessment models. This serves to connect the terminology in use in piping assessments to that of more generic hydrological and geological mapping of areas such as the Rhine-Meuse delta plain.

2.1. Piping process and assessment

In this study we consider piping as the combined result of three different processes: *bursting, heave* and *backward erosion* (Richards and Reddy, 2007). During periods of high discharge, high water levels in the embanked river drive groundwater flow and pressure gradients in the shallow ($\sim < 4$ m) sandy aquifer underneath the dike. These pressure gradients may result in the build-up of pore pressure in the subsoil at the land-side of the dike, which can cause failure of the aquitard overburden layer (*bursting*), starting a concentrated outflow of water. If the vertical outflow gradient exceeds the particle-entrainment critical threshold value (e.g. Shields, 1936), aquifer sand grains will be transported

upwards (*heave*) creating sand boils at the surface (Kolb, 1975; Bridle and Fell, 2013). Bursting and heave are required preconditions for the initiation of *backward erosion* as a third process, creating small open conduits (i.e. pipes), propagating in opposite flow direction towards the river, underneath the dike. Backward erosion and pipe formation occur in the sandy aquifer top, at the interface with the finer grained overburden.

Currently, the Dutch standardized safety assessments of piping (Kruse and Hijma, 2015) use the Sellmeijer equations (Sellmeijer, 1988; Sellmeijer, 2006) that calculate the backward erosion potential at specific water levels (Fig. 2). The parameters in these equations include: thickness of sandy and overburden deposits ($D_{aquifer}$ and $D_{overburden}$) (architectural information), grain size permeability (D_{70} and K_{sat}) of the sandy deposits (composition information) and a correction factor for flow friction within the overburden. Note that D_{70} is a parameter quantified from grain size distributions obtained from sieving or laser diffraction measurements on materials used in lab scale experiments and on selected field samples, while routine geological description of shallow boreholes and definitions of texture class descriptions estimate D_{50} and some indication of sorting (e.g. USDA - Soil Survey Division Staff, 1993; NEN 5104: 1989/C1:1990 nl, 1990), and likewise in our dataset UU-LLG, Cohen et al., 2017a). Variations in D_{50} directly reflect changes in the grain-size distributions and are regarded to closely approximate values and variations of the D_{70} and K_{sat} parameters that the piping risk calculations take in (Kanning, 2012; Dirkx et al., 2020).

2.2. Linking geological mapping to piping parameters

The Holocene Rhine-Meuse delta is situated in the southern part of the gradually subsiding North Sea sedimentary basin (Ziegler, 1994; Kooi et al., 1998). Climate and sea-level changes over the last few million years, besides basin and local fault zone tectonic subsidence, created accommodation space and variations in local surface gradient, resulting in changing fluvial patterns and a complex heterogeneous sequence of gravely sandy aquifers alternating with confining clayey layers, up to hundreds of meters thick (e.g. Van Balen et al., 2005; Busschers et al., 2007). The upper aquifer consists of widespread sandy deposits of Middle to Late Pleistocene age (*pre-deltaic sands*) which are overlain by the Holocene deltaic wedge (Fig. 1B). The latter is a complex confining layer (Bierkens, 1994; Weerts, 1996), mostly composed of aquitard clays and peats but dissected by channel-belt sand bodies (*deltaic sands*) from past and present river systems (Berendsen and Stouthamer, 2000; Fig. 2), that in majority connect to the upper aquifer. The ribbon-shaped sand bodies thus act as shallow-depth aquifers. Many stretches of modern river dikes across the delta are underlain by these fossil river channel belts and their compositional properties govern the opportunities of formation and progradation of pipes (Kanning, 2012; Robbins and Van Beek, 2015). Furthermore, where channel belts connect to the deeper aquifer deposits this drastically increases the effective aquifer thickness, which is a relevant hydrological boundary condition for piping (Sellmeijer, 1988). In the Rhine-Meuse delta, main channel belts have a typical thickness of 6–7 m (Gouw, 2008), whereas the deltaic wedge in downstream direction reaches thicknesses over 10 m (Fig. 1B). The implication is that in downstream a direction, channel belts are increasingly less connected to the upper main aquifer. Especially the younger generations of channel belts downstream in the delta lose their direct hydrological connection.

Still, at locations where these younger generations channel belts intersect with older and deeper channel belts or partly reoccupy them, their shallower sand bodies locally make a hydrological connection to the deeper aquifer in downstream sectors (indirect connection).

3. Geological development and subsurface architecture

In order to better grasp the spatial variability of subsurface characteristics we here characterize the different types of sandy deposits in the

Formula used in Dike assesments

Linking piping parameters to geological mapping

Sellmeijer equations for calculating backward erosion

$$F_{resistance} = \eta \, \frac{\gamma_{sub.particles}}{\gamma_{water}} \tan \Phi$$

$$F_{scale} = \frac{d_{70.m}}{\sqrt[3]{\kappa L}} \left(\frac{D_{70}}{d_{70.m}} \right)^{0.4}$$

$$\kappa = \frac{\nu_{water}}{g} K_{sat}$$

$$F_{geometry} = 0.91 \left(\frac{D_{aquifer}}{L} \right)^{\frac{0.28}{\left(\frac{D_{aquifer}}{L} \right)^{2.8} -1} + 0.04}$$

(for detailed explanation see Sellmeijer 2016)

Architectural parameters: $D_{aquifer}$, $D_{cover\,layer}$

Lithological parameters: D_{70} , K_{sat}

Deltaic (complex confining layer)
- Channel-belt sand deposits (ribbon sands)
- Clayey overbank deposits
- Autochthonous organics

Pre deltaic (upper aquifer)
- Aeolian River dunes deposits
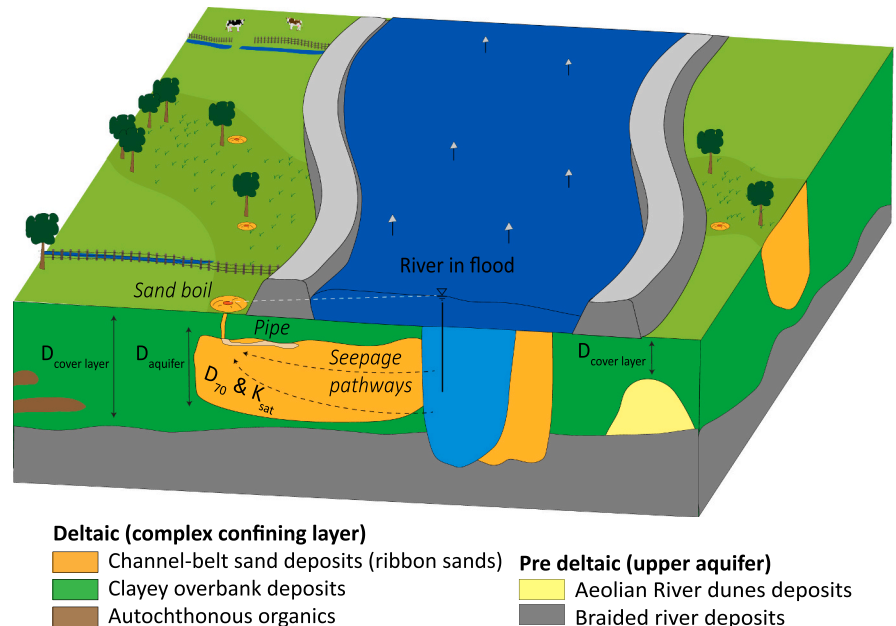- Braided river deposits

Fig. 2. Conceptual block diagram showing architectural setting of deltaic and pre-deltaic sands, and their relation with parameterization incorporated in the Sellmeijer formula for evaluation of backward erosion potential ('piping').

Rhine-Meuse delta setting, connected to their depositional environment and genesis. This provides a basis for regionalized geological subdivision of the study area used in the further paper.

3.1. Shallow deltaic deposits (complex confining layer)

The Holocene deltaic wedge is about 1 m thick near the delta apex and thickens to over 10 m in downstream direction of the study area (e. g. Cohen et al., 2005; Gouw, 2008). Besides the channel-belt sand bodies, its architecture further contains elements of overbank deposits derived from these channels (in proximal and distal setting variants) and autochthonous organics (Fig. 1B). The deltaic wedge is post-glacial and formed after main stages of eustatic sea-level rise by 9000 yr BP had caused inundation of inner shelf areas of the southern North Sea (e.g. Hijma and Cohen, 2019). Between 8500 and 7500 yr. BP, a barrier coastline established in front of the then joint Rhine-Meuse river mouth. Rapid relative sea-level rise until ~6000 yr. BP and associated rise of inland river water and groundwater levels created abundant new accommodation space that was filled with sediment, waterand organics (Berendsen and Stouthamer, 2000;). From 8500 years onwards, this is seen as a progressive inland shift of deltaic onlap over the pre-deltaic valley surface, reaching 100–150 km inland of contemporary coast lines (Stouthamer and Berendsen, 2001; Stouthamer et al., 2011).

By 6000 yr. BP, rates of relative sea-level rise had much decreased and a so-called high stand situation was reached in which the position of the coast line stabilized (Beets and Van der Spek, 2000; Hijma and Cohen, 2019). Still, regional land subsidence and compaction of soft deltaic sediments and organics continued to create accommodation space (Cohen et al., 2005; Van Asselen et al., 2017), thus allowing continued trapping of sediment in back-barrier areas, in tidal-basins downstream and fluvial flood basins inland. This helped a barrier island coastline to mature into an elongated beach barrier system allowing for a phase of extensive peat formation in the lower and central parts of the delta, that would continue until ~2000 yr. BP (e.g. Pierik et al., 2018). The extensive marshes, fens and swamps of the freshened back-barrier plain limited the formation of new channels in the lower delta plain (Berendsen and Stouthamer, 2000).

Prehistoric deforestation in the German hinterland by 3000 yr. BP led to a 60–100% increase of the suspended (fine) sediment load of the Rhine system. This is regarded to have driven reorganization of the delta apex region, where new avulsions occurred and overbank deposition enhanced (Gouw and Erkens, 2007; Erkens and Cohen, 2009), as well as in the lower delta where new branches formed, crossing the deforested and cultivated lower deltaic peat land (Pierik et al., 2018). The last major avulsion took place approximately 1400 yr BP (Makaske et al., 2008; Cohen et al., 2009, 2012) and initiated the IJssel branch which diverted northward, upstream in the study area.

In the late Middle Ages, increased population and socio-economic and technological developments made inhabitants of the Rhine–Meuse delta to construct dikes along all major rivers in the 11th to 12th cy AD in the west and in the 13th–14th cy AD in the apex and IJssel areas (Hesselink et al., 2003). The construction of dikes, resulting in ca. 1-km wide 'embanked floodplain' zones flanking the rivers, impacted channel hydraulic and overbank sedimentation characteristics of the rivers: it compartmented the former floodplain and restricted the overbank area where flood sedimentation was allowed to continue (e.g. Middelkoop, 1997).

As a result of the geological development, fluvial channel-belt deposits occur throughout the delta subsurface, with older generations found at greater depth. Within the study area, four generations (>5000 cal. yr. BP, 5000–3000 cal. yr. BP, 3000–800 cal. yr. BP and < 800 cal. yr. BP) of channel belts can be distinguished based on changing boundary conditions during their formation (Table 1). Owing to aggradation and avulsion, younger generations of channel-belt sand bodies regularly occur stacked (i.e. amalgamated cf. Gouw, 2008) to older ones. This is particularly true for the narrow proximal part of the delta plain and the northern and southern delta margins. In the wider distal delta plain, channels belts occur more isolated (Gouw and Erkens, 2007; Stouthamer et al., 2011).

3.2. Deeper pre-deltaic sands (upper confined aquifer)

The pre-deltaic sands comprise the upper most part of the aquifer underlying the Holocene deltaic wedge (Fig. 1B and Fig. 2). Below most

Table 1

Subdivision criteria for various (pre-)deltaic geogenetic units and impacts on architectural and lithological characteristics.

Geogenetic units	Subdivision criteria	
(a)-(i)	Architectural characteristics	Lithological characteristics
Deltaic deposits		
Aggrading channel belts	Isolated, stacked ribbon sands	Heterolithic sands, fining upward tops
Age grouping (last functioning):		
(a) 800 cal. yr. BP. - Present	Constrained by artificial levees	Confined overbank sedimentation
(b) 3000–800 cal. yr BP	*Re*-expanding branch network	Increasing fine sediment delivery
(c) 5000–3000 cal. yr BP	Delta rim trunk channels	
(d) > 5000 cal. yr BP	*Backstepping avulsions under decelerating relative sea level rise	
	*Thick overbank deposits	
	owing to drowning under decelerating relative sea level rise	
Pre-deltaic deposits		
(e) Braided river deposits	Spatially extensive (braid plain)	Coarse sandy/gravelly sediments
(f) Early Holocene channel belts	Narrower belt in incised position	Reworking source material
(g) Cover sands	Wide spread units (blanket), shallow depth, flanking braid plains	Wind-blown, fine grained, well-sorted sands
(h) Inland dunes	Local sand bodies, flanking a contemporary riverine source	Wind-blown, medium grained, moderately sorted
(i) Local alluvium	Local fans, associated to bounding relief	Relative coarse grained

of the study area, these are relatively coarse-grained fluvial deposits left by the Rhine and Meuse rivers in the second half of the Last Glacial (50,000–15,000 years BP; Busschers et al., 2007). During this period cold-stage braided rivers developed under discharge and sediment transport conditions of seasonal snow smelt, sparse vegetation cover and relatively strong winds (e.g. Kasse, 1997; Hoek, 1997). The Rhine and Meuse braided river channels had their confluence in the study area. Several larger river channels functioned side by side and the braid belt shifted laterally, leaving a broad valley floor: some 60-km wide in the east and 25-km in the west of the study area (Busschers et al., 2007; Hijma et al., 2009; Cohen et al., 2012). To the north and south, older fluvial and relict ice-marginal landforms drained by local snow-smelt rivers bordered the Rhine-Meuse palaeovalley. Due to highly variable discharges, the glacial braided-river systems produced complex depositional sequences, predominantly consisting of coarse material ranging from coarse sand to gravel deposits (Busschers et al., 2007).

Stormy conditions in barren landscapes under subarctic climate conditions resulted in widespread aeolian depositional activity in western and central Europe (Kasse, 1997;), evident from extensive blankets of cover sands found over terrains adjacent to the Rhine-Meuse palaeovalley. The cover sands mainly consist of locally sourced sediments and are generally well sorted and relatively fine grained (grain-sizes range between 150 and 420 μm; Schwan, 1986 – see also section 5.1.2). In the north-east of the study area (notably along the young IJssel branch, see above), cover-sand deposits are found at relatively shallow depths, compared to the braided deposits mentioned above, and at the surface.

At the very end of the Last Glacial (during the Younger Dryas cold spell, 12,500–11,700 years BP), considerably increased amounts of sand were blown out of the seasonally dry braided river beds, forming high inland dune complexes on higher-elevated remnants of the former braid plain (e.g. Berendsen et al., 1995; Berendsen and Stouthamer, 2000). In

the downstream part of the study area, these fossil inland dunes have become buried by flood basin deposits when the deltaic wedge accumulated. Their very tops are locally found outcropping and subcropping. In the upstream parts of the delta the dune topography is still emerging above the thinner deltaic wedge. Compared to cover sands, the inland dune sands are slightly coarser grained and less well rounded (typical grain sizes ranging between 210 and 420 μm; Weerts, 1996 – see also section 5.1.2).

During the Lateglacial and Early Holocene, 14,000–9000 yrs. BP, climate change altered the hydrological regime and conditions for vegetation in the study area and the river hinterland, which triggered a fluvial style change in the Rhine-Meuse valley. The active braid belt width of the rivers began to contract. Large parts of the braid plain were abandoned and became floodplain terraces, while within km-wide winding belts the river was meandering and continued to rework the braid-plain inherited sandy deposits (Berendsen and Stouthamer, 2000; Busschers et al., 2007). Importantly, this climatically triggered fluvial style change in the valley was completed before proceeding sea-level rise transformed it into a deltaic environment (Hijma and Cohen, 2019, Stouthamer et al., 2011). Based on their geological development and subsurface architecture characteristics we distinguish four units of pre-deltaic sandy deposits: i) braided river deposits, ii) incising meandering channel deposits, iii) wind-blown cover sand deposits and iv) wind-blown inland dune deposits (Table 1).

4. Methods

4.1. Compiling the geogenetic typology map

The spatial extent of the various (pre-)deltaic sandy deposits was derived from existing geological maps, especially those available in digital data set form (Datasets A-E, Table 2). We here describe how we

Table 2

Generic geologic mappings containing spatial extent of various (pre-)deltaic environments in ascending order is order of processing, descending order is order of stratigraphic overruling.

| Depositional environment	Datasets	Reference, version
Early Holocene channel belts (pre-deltaic)	Dataset A: Basemap RMD Palaeogeography (valley layer)	Cohen et al. (2012); modified 2015 (Cohen et al., 2017)
Braided river deposits (pre-deltaic, Late Pleistocene)	Dataset A: Basemap RMD Palaeogeography (valley layer)	Cohen et al., 2012; modified 2015 (Cohen et al., 2017)
Cover sands (pre-deltaic, Late Pleistocene)	Dataset B: Zand in Banen / Dataset C: GEOTOP	Cohen et al. (2009); Van der Meulen et al. (2013)
Inland dunes (pre-deltaic, Late Pleistocene)	Dataset D: Verwachting in Lagen	Cohen et al. (2017)
Deltaic channel belts (Middle and Late Holocene)	Dataset E: Basemap RMD (delta channel belt layer)	Cohen et al. (2012); modified 2015 (Cohen et al., 2017)
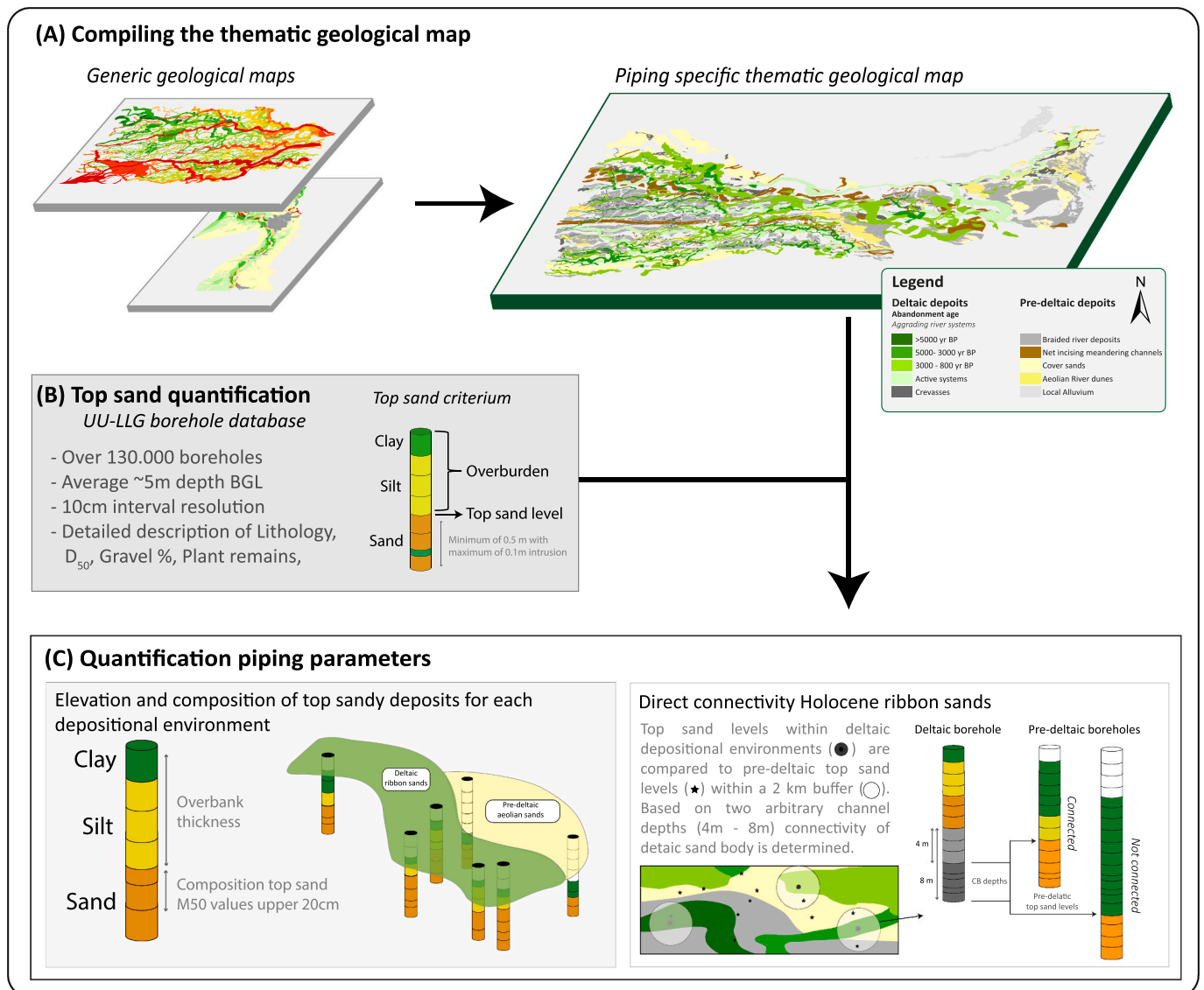
Fig. 3. Schematic workflow showing backward erosion parameters quantification steps. (A) Existing geological maps containing spatial extent of the various (pre-) deltaic sandy deposits merged in a thematic geological map for use in quantifying piping parameters. (B) Main characteristics UU-LLG subsurface database (Cohen et al., 2017a) and Top sand criteria used in borehole queries. (C) Quantification of piping parameters (overburden thickness, D_{50} top sand) and direct connectivity of Holocene ribbon sands.

combined information from existing digital geological maps, to what we call a geogenetic typology map (i.e. geological framework), that distinguishes areas of substrate of different genesis and inherent lithological characteristics (Fig. 3A). The zonation that results is reasoned to be relevant for the assessment of piping susceptibility (section 2), echoes insights from past geological mapping (section 3), and will be used to aggregate borehole-database results (section 4.2 and beyond).

Mapped information regarding the pre-deltaic sand units *braided river deposits* and *early Holocene channel belt deposits* was retrieved from geological mapping by Utrecht University (Dataset A - Cohen et al., 2012, modified 2015). This source (1) contains the extent of the fluvial terraces and channel belts that make up the palaeovalley surface underlying the Holocene deltaic wedge and (2) gives the depositional age of the channel sands. The youngest fluvial activity of the palaeovalley maps out as an incised meander belt, queried in GIS as the area with river activity younger than 11,600 cal. yr. BP, and relabelled *early Holocene channel belt deposits*. Remaining palaeovalley floor was labelled *braided river deposits*. The spatial extent of cover sands was reconstructed by merging two datasets: Dataset B (Geological Survey; Van der Meulen

et al., 2013; Cohen et al., 2017) and Dataset C (Utrecht University, Cohen et al., 2009). Datasets B and C are complementary and together these cover the entire study area. In overlapping areas in the east of the study area, the higher resolution mapping in Dataset C was given preference over Dataset B (geological survey mapping is in revision for that subarea). Dataset D (Cohen et al., 2017) was used to provide the spatial extent of inland aeolian dunes as a separate type of wind-blown deposits.

The spatial extent of deltaic *channel belts* and their grouping into generations based on age was taken from channel belt mapping by Utrecht University (Dataset E – Cohen et al., 2012). From this mapping we also derived the depth of the top of the channel belt sands and downstream gradients therein. The final map was obtained after several iterative rounds using GIS-methodologies to ensure that age-reconstructions are spatially consistent (Berendsen and Stouthamer, 2000). We grouped the channel belts into the four generations. Merging and dissolving these datasets was done in compliance with the stratigraphic order of the various depositional units (cf. Pierik et al., 2016; Cohen et al., 2017). In these operations with datasets A-E, polygons representing younger generations in one data set replace those of older
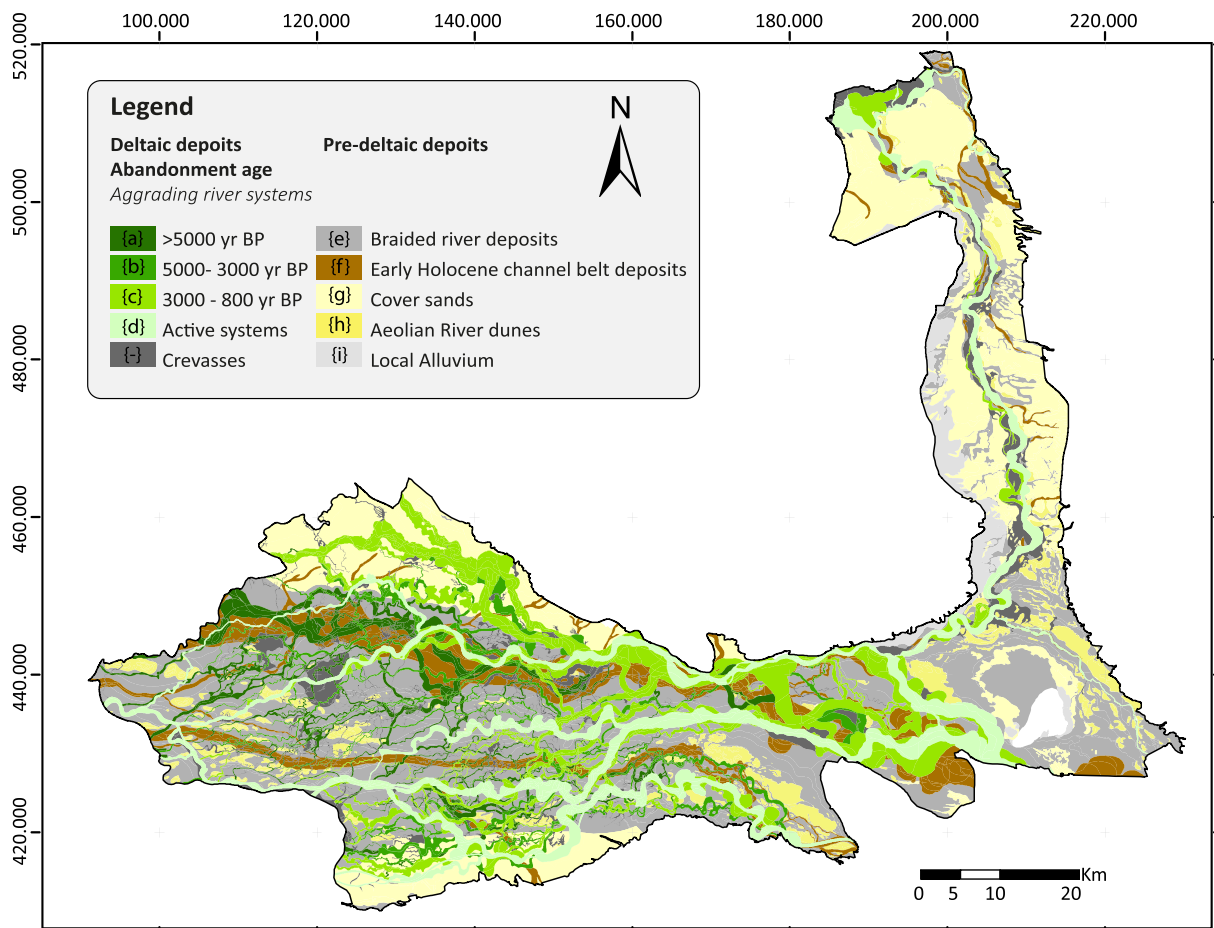
Fig. 4. Thematic geological map with geogenetic typology of the shallowest sand encountered, relevant to quantifying piping parameters in the Rhine-Meuse delta. The map shows distribution and extent of deltaic sands (four units, see also Table 1) and pre-deltaic sandy substrate (five units, see also Table 1). Soft-soil deltaic overburden burying the sandy strata is not indicated (i.e. left transparent) on this map.

generations in another data set (Table 2). This results in a geogenetic typology map that represents the depositional environment and age of the first encountered sandy deposits (Fig. 4).

Table 3
Primary and secondary subdivisions criteria for regional subdivision study area.

Zonation of study area		Subdivision reasons (expectations)
Zone A		Large width 'unconfined' Rhine-Meuse delta (*E*-W trends)
		Channel belt network: mainly isolated relatively narrow sand bodies
Zone B		Large width 'unconfined' Rhine-Meuse delta (E-W trends)
	B1	Depth and nature of pre-deltaic substrate: Cover sands at relatively shallow depth (reworking impacts)
	B2	Depth and nature of pre-deltaic substrate: Palaeovalley sands, relatively deep
		Channel belt network: long-active trunk sand bodies (central reference situation)
	B3	Depth and nature of pre-deltaic substrate: Cover sands at relatively shallow depth (reworking impacts)
Zone C		Narrow 'confined' part of Rhine-Meuse delta (E-W trends; Reworking impacts)
	C1	Rhine part (effects of larger bed load and reworking capacity)
	C2	Meuse part (smaller bed load and reworking capacity)
Zone D		IJssel branch (S—N trends; Reworking impacts)
	D1	Depth and slope of the Pleistocene substrate in opposite direction
	D2	Depth and slope of the Pleistocene substrate in flow direction

4.2. Quantifying architectural and lithological properties

4.2.1. Approach & materials

Information on architectural and lithological characteristics of the delta subsurface was obtained from the UU-LLG digital database of the Rhine-Meuse delta (Berendsen and Stouthamer, 2001; Cohen et al., 2017a). This database contains detailed lithological descriptions (10-cm vertical resolution) for over 130,000 hand-cored, field-logged boreholes, in majority terminating in either deltaic sands or reaching the pre-deltaic sands. The key logged property retrieved from these data for this study is the texture or 'litho-class' (coded cf. de Bakker and Schelling, 1966; Berendsen and Stouthamer, 2001). In addition, for sandy deposits the median grain size class (D_{50}) has been logged. We first queried the database on the following information for individual cores (Fig. 3B - architectural: depth top of sand body and thickness of confining overburden; lithological: median grain size of sand).

Next we aggregated this information by grouping boreholes and calculating descriptive statistics based on location overlayed on the geogenetic map (Fig. 3C). As a second grouping criteria we introduced a regional zonation (Table 3; Appendix A; zones A, B1–3, C1–2, D1–2), based on architectural understanding of the deltaic wedge (see section 3). To produce longitudinal trend plots for grain size and overburden thickness, some further basic aggregation techniques were deployed: we used a 2-km long moving-window over the national coordinate grid thus averaging cross-valley variance (central delta: *E*-W, IJssel branch: *Z*-N) (Fig. 6). All longitudinal transects were cut off where less than 10 boreholes remained in the 2-km window.

4.2.2. Depth of the top of the sand bodies and Overburden Thickness

The depth (m - surface level) of the top of the sand bodies was obtained by querying the UU-LLG lithological descriptions. The *top of the sand* bodies is defined as the depth below the terrain surface where the top of the shallowest layer of sand and/or gravel with a minimum thickness of 50 cm occurs, tolerating an interrupting layer of other material with a maximum thickness of 10 cm (Fig. 3B, Appendix A). The 50-cm thickness requirement was chosen to exclude (i) thinner sand layers which are part of the confining overburden (and not susceptible to backward erosion / piping) and (ii) borehole records with insufficient penetration depth to decide whether the first sand encountered is the top of the sand body or an intercalation within the overburden. The *thickness of the confining overburden* follows from the Top of Sand identification. It is defined as the thickness of the deposits overlying it up to the surface (Fig. 3B). We transposed the raw results by deploying a projection procedure that adds additional fictive overburden thickness to observed at distance inland from dikes (Appendix B). Such corrects regional differences in surface lowering due to anthropogenic compaction of soft deltaic sediments and organics (section 3.1), which is needed to use regional data as representative quantifications of overburden thickness at the position of dikes (Fig. 6).

4.2.3. Characteristic D_{50} grain sizes top of sand

Multiple database query actions were performed to prepare the UU-LLG database records for querying a representative central $D_{50 \text{ top sand}}$ value for each unit of the geogenetic map (Appendix C), that allows for description and investigation of spatial trends and patterns in median grain sizes throughout the study area. After these conversions, the average of the D_{50} values queried for the upper 20 cm of the sand bodies was used in the further analysis. From the resulting dataset of field-estimated $D_{50 \text{ top sand}}$ values, we report the mean values per geological unit and region. We included the standard error, allowing us to evaluate if means differ significantly between units and subregions. The considerable spread in individual values (variance) is communicated as violin plots on a logarithmic axis (Fig. 5). We also present the data in longitudinal plots (Figs. 6 and 7), together with such plots for overburden thickness. Note that $D_{50 \text{ top sand}}$ should be regarded a lower end estimate for a D_{50} representative for an entire deltaic channel sand body, as these systems are generally fining upward (e.g. Allen, 1970).

4.2.4. Aquifer thickness and connectivity

Because the majority of UU-LLG boreholes were terminated when hitting the upper few decimetres of the channel belt deposits (top of sand), data-driven identification of locations where channel belts have a *direct connection* with pre-deltaic deposits is challenging. Predictive approaches to connectedness using characteristic values of channel belt thicknesses from local case studies are also tricky because, as the same case studies reveal the geometry of deltaic channel-belt bases to be highly irregular (Gouw and Berendsen, 2007; Makaske et al., 2007).

Hence, the *direct connectivity* was determined by comparing the vertical difference between top-of-sand in each channel belt (deltaic) borehole and top-of-sand levels of nearby (within 2 km) pre-deltaic boreholes and evaluated whether the difference exceeds an arbitrary channel minimum and maximum channel belt sand thickness of 4 resp. 8 m (i.e. positive connectivity evaluation Fig. 3C). The connectivity fraction (CF) was calculated by dividing the total number of pre-deltaic cores within the 2 km buffer, by the amount of pre-deltaic cores with a positive connectivity evaluation. Regional aggregation of these numbers gives an indication of the connectivity probability of channel belts for each specific region. Assessing the locations where *indirect connection* occurred owing to stacking of multiple generations of deltaic channel belts (amalgamated, e.g. Gouw, 2008), was more straightforward because such information is contained in the topology of Dataset E (Table 2) and could be queried directly.

5. Variability in architectural and lithological properties

Here we describe the architectural and lithological characteristics of the sand body types in each of subregion (our predefined zones) of the delta, and evaluate to what extent that aggregation results in a reduced within-zone variance (Fig. 5).

5.1. Regional variability across depositional environments

Zone A is situated in the wide downstream part of the Rhine-Meuse delta (Fig. 6), where the deltaic wedge is thick and spans the last 8000 years (Fig. 1). Relatively narrow deltaic channels cover 31% of this zone and older channel belt generations are relatively abundant. More than 69% of this zone sand is first encountered below the deltaic wedge. These pre-deltaic substrate deposits consist mainly of braided river and early Holocene channel belt deposits (Fig. 5). Zone B represents the central part of the delta plain and stretches westward along the rims of the west-central delta plain (Fig. 5). In Zones B1 and B3, between channel belts (B1: 37%, B3: 36% of area), the substrate consists predominantly of cover sands (B1: 58%; B3: 59%), whereas in Zone B2 it is similar to Zone A (braided river deposits 29%: early Holocene channel belts: 14%; deltaic channel belts: 51%). Deltaic channel belts are, however relatively wider than within Zone A. Older generations cluster in Zone B2, later generations in marginal zones B1 and B3, while youngest generations spread out evenly over all three subzones (Fig. 5). Zone C is the inland upper delta plain and is subdivided in a Rhine (C1) and Meuse (C2) subzone. Fossil inland dune areas characterize the area separating these two zones (Figs. 4 and 5). In zone C1, deltaic channel belt deposits cover 49% of the area, compared to 29% in zone C2. Results for the oldest generations of deltaic channel belts are not generated in Zone C, due to delayed aggradation owing to underlying pre-deltaic topography (Fig. 1B and 4). Zone D comprises the delta-apex floodplain and the young IJssel channel belt (subzone D1), that escaped the earlier used delta plain and annexed a relative wide northward stretching valley (subzone D2). Channel belt sands of the single new river branch occur over modest area (D1: 16%; D2: 19%), whereas predeltaic cover sands, inland dunes and braided river deposits occur widely (D1: 84%; D2: 81%) and at shallow depths (Figs. 4 and 5).

5.1.1. Deltaic deposits

In the centre of the lower delta plain (Zones A and B2), $D_{50 \text{ top sand}}$ values change with channel belt generation, with coarsest sediments (Zone A: $\mu = 293 \pm 7$ μm, Zone B2: $\mu = 327 \pm 5$ μm) found within youngest generation channel belts. In the upper delta plain, $D_{50 \text{ top sand}}$ values show partly deviating trends. Within Zone C1 (Rhine), no shift with channel belt generations and $D_{50 \text{ top sand}}$ values is seen. Results for Zone C2 (Meuse), as in the downstream zones, do show the coarsening of $D_{50 \text{ top sand}}$ with younger channel belt generations. Absolute values for $D_{50 \text{ top sand}}$ in Zone C2 are below those of Zone C1, the difference increases for older generations ($\Delta D_{50 \text{ top sand}}$: {d} 18 μm, {c} 35 μm, {b} 76 μm and {a} 88 μm). That channel belt sands of the Meuse are slightly finer grained at their top, can also be observed from comparing zone B3 (Meuse) to and B2 (Rhine and Meuse). The $D_{50 \text{ top sand}}$ of channel belts is also relatively lower (finer grained) in delta rim areas with abundant wind-blown deposits in the pre-deltaic substrate (i.e. in zone B1, B3, D1, D2). The difference with values in Zones A, B2 and C1 is ~40 μm. $D_{50 \text{ top sand}}$ values in these rim areas also show less variance than the central delta areas underlain by deeper coarser grained pre-deltaic deposits (violin plots in Fig. 5).

Overburden thickness decreases for younger channel belt generations (Fig. 5), in correspondence with the aggradation history of the Holocene deltaic wedge (Section 3.1). Thickness is largest over older channel belt generations, and more or less comparable for the younger two generations (Fig. 5). Meter-scale variation seen in the oldest generation (>5000 cal. yr. BP) is due to the considerable rates of sea-level rise at that time (e.g. Stouthamer et al., 2011). Submeter-scale
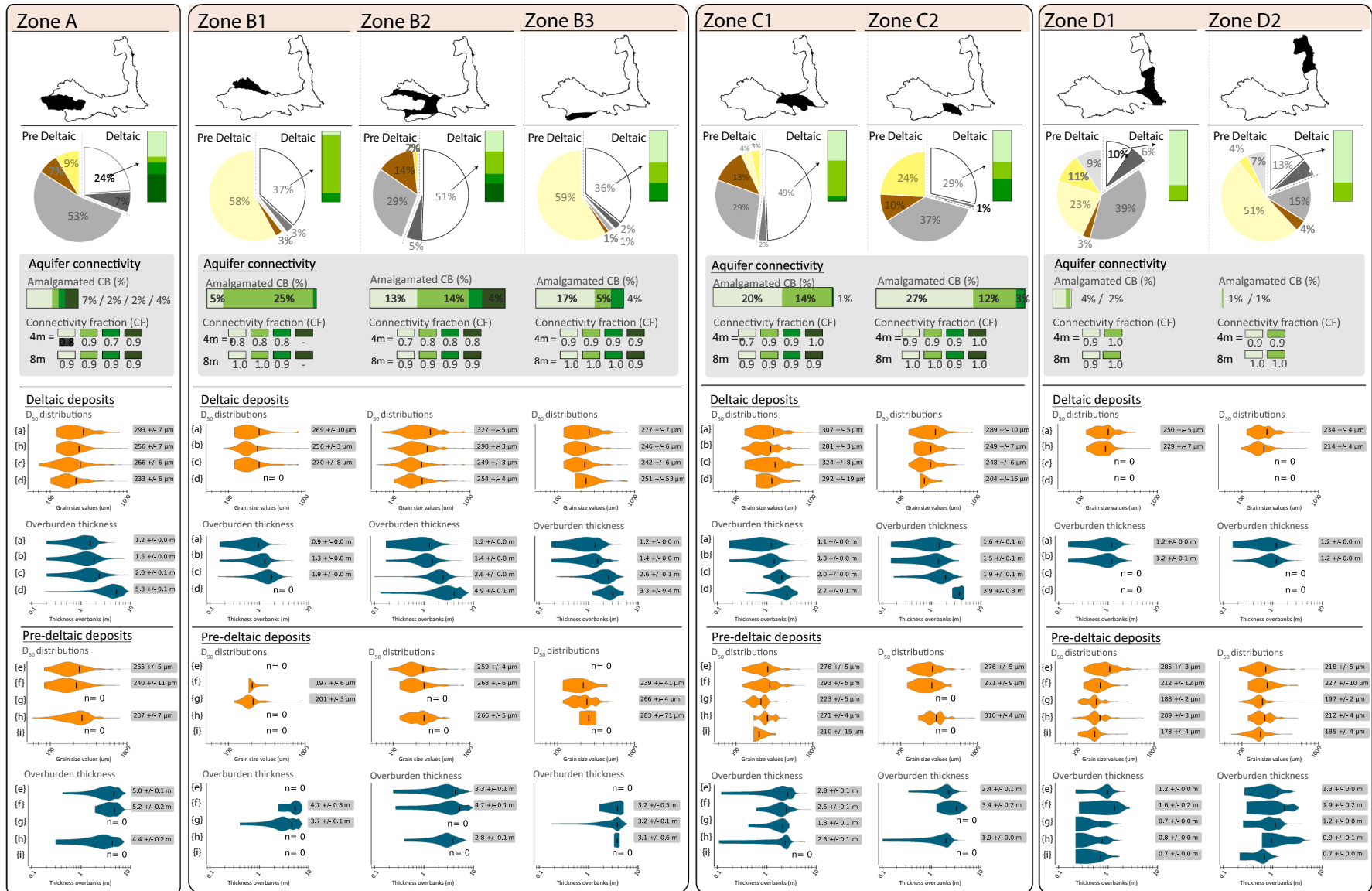
Fig. 5. Multipanel reference chart of geologically derived quantifications of piping parameters for the Rhine-Meuse delta, based on Utrecht University mapping and borehole data (architectural resp. lithological properties). Rows split results for deltaic channel belts from those fore pre-deltaic aquifer sands, columns split the results regionally. Pie-charts give areal percentages (color scheme is the same as Fig. 4). Aquifer connectivity is represented by percentage amalgamated channel belts (CB) and connectivity factors (CF). Violin plots (orange = Top-of-Sand D_{50} values in μm, blue = overburden thickness in m; black bars: mean value) show value distribution, and report mean values and the standard error of this mean (queried from borehole data). (For interpretation of the references to color in this figure legend, the reader is referred to the web version of this article.)

variation in overbank deposit thickness, seen in the younger generations, is attributed to local elevation differences due to point bar morphology of deltaic sand bodies. For the youngest generation, this submeter-scale variation, is caused by embankment of the floodplain restricting the depositional area (section 3.1). Compared to Zone B2, Zone B1 shows relatively thinner overburden deposits (Δ 0.5 m) for the second oldest generation channel belts (Fig. 5). Younger generation channel belts from when the Rhine trunk system had fully established through area B1 (e.g. Stouthamer et al., 2011), do not show this difference. Overburden thickness on top of the IJssel channel belt in Zones D1 and D2 is significantly less than in the central delta, and ranges between 0.5 and 3 m, which can be attributed to the short span of activity of the river IJssel.

Connectivity of deltaic sands to the upper aquifer decreases in downstream direction. Regarding direct connection, the connectivity fraction CF values for 4 m are the most sensitive in showing this. Values of upstream zones for all four channel belt generations lie close to 1 (zone C1: 0.79, 0.92, 0.97, 1.0 and zone C2: 0.98, 0.99, 0.95, 1.0) while downstream zones (A, B1, B2, B3) show values that are ~0.1 lower (Fig. 5). When assuming 8 m thick channel belt deposits, the CF lies close to 1 across the entire study area (Fig. 5).

In contrast to direct connection and CF values, scores for indirect connectivity are higher for younger generations of deltaic channel belts, as younger channel belts dissected and reoccupied older ones, reworking their deposits. The percentage of deltaic sand body area that is amalgamated (Fig. 5), is greatest in the upstream delta (Zones C1: 35%, C2: 42%). This is due to the relief-bounded relatively narrow width of this part of the delta plain, which forces good-sized branches spawned by avulsions this high up in the delta (apex-bifurcations) to reoccupy and dissect equally good-sized precursors frequently (e.g. Stouthamer et al., 2011). In the widened central delta plain (Zones A, B1, B2 and B3), the percentage of stacked channel belt area drops (Zones B1: 31%, B2: 38%, B3: 26% - Fig. 5: grey panels). The lower delta plain (Zone A) has the lowest values (2–7%), owing to the more isolated occurrence of channel belts this far downstream (see section 3).

5.1.2. Pre-deltaic deposits

Below the central lower delta plain (Zone A), the $D_{50 \text{ top sand}}$ values of the top of the upper aquifer are slightly finer grained ($\Delta D_{50 \text{ top sand}} \sim 25$ μm) in the Early Holocene channel deposits (i.e. the zone longest reworked by meandering rivers prior to deltaic formation), compared to that of the braided river deposits (abandoned and left as terraces during the late glacial (Fig. 5). In other parts of the delta (Zones B1–3, C1 and C2), such a difference is less apparent or even inverted (Fig. 5). Below the northern and southern delta rims (Zone B1 and B3), the presence of cover sands shifts $D_{50 \text{ top sand}}$ to finer grained values. The violin plots (Fig. 5) also reveal reduced spread in the values, subscribing established notions that wind-blown cover sands are intrinsically 'better sorted' than river-lain pre-deltaic and deltaic sands (section 3). Cover sand deposits in northwestern Zone B1, and easterly Zones D1 and D2, despite their separation distance and differences in antecedent geological history, have comparable mean grain-size values ($D_{50 \text{ top sand}} = 190$ to 200 μm) and variability. In comparison, $D_{50 \text{ top sand}}$ for cover sand in Zone B3 to the south is coarser (266 ± 4 μm) and shows greater variability (Fig. 5). For inland dunes, $D_{50 \text{ top sand}}$ values for are modestly greater than for cover sand ($\Delta D_{50 \text{ top sand}} \sim 20$ μm). In Zones C1 and C2, the violin plots for inland dunes show a remarkable bimodal distribution (Fig. 5), potentially echoing to local bed composition of the braided rivers (smoothed out in the aggregated results of Fig. 5; but see section 5.2 and Fig. 6 below) that were the source areas for the dune fields in the pre-deltaic situation (e.g. Kasse et al., 1995; Berendsen et al., 1995). In zone D (river IJssel), for similar reasons of local source area variation and gradual braid plain abandonment particularities (e.g. Cohen et al., 2009), $D_{50 \text{ top sand}}$ for the inland dunes is ~80 μm lower than in Zone C (Fig. 5) and consequently closer to $D_{50 \text{ top sand}}$ for cover sand substrate.

Downstream trends of overburden thicknesses over inland dunes

show an increase from ~1 m typically in the upstream zones to ~4 m on average in the downstream zones (Fig. 5). In addition, owing to their irregular morphology, throughout the study area overburden thickness over the fossil inland dunes shows larger variance than for the other pre-deltaic geogenetic units which have smoother buried relief. Mean overburden thickness for delta flank regions (Zones B1 and B3) is about 1 m less than in the equivalent central zone (Zone B2). It is thickest over the Early Holocene channel deposits: over that deepest incised part of pre-deltaic valley floor the overburden on average is 0.5 to 1.0 m thicker than over the surrounding braided river areas (Fig. 5. Along the IJssel branch (Zones D1 and D2), overburden thickness is limited. Values range between 0.5 and 2 m across the various pre-deltaic units, similar to overburden thickness over the IJssel channel belt itself (Fig. 5).

5.2. Longitudinal trends in architectural and lithological properties

5.2.1. Main delta plain (E-W downstream trends)

Lumped and generation-separated longitudinal plots of $D_{50 \text{ top sand}}$ for the Rhine-Meuse channel belt sand bodies show clear regional longitudinal trends, albeit with superimposed local variations (Fig. 6 – Ia/b, IIa/b). Regional downstream fining trends are expected for bed sediments of deltaic and pre-deltaic riverine units, as outcome of selective transport processes (i.e. preferential transport of the finer sand fractions downstream) known to operate in the lower reaches of Rhine and Meuse (e.g. Frings et al., 2019). In our grainsize results for the very top of fossil bed deposits, however, a clear downstream fining trend only starts halfway the study area (downstream of X = 160 km; Fig. 6 – Ia), where deltaic branches leave the relatively narrow delta plain of Zone C and the widened delta plain of Zones A + B. From there, the moving-window averaged $D_{50 \text{ top sand}}$ for all generations of deltaic sand bodies lumped drops from ~300 to ~200 μm. This downstream fining trend is more pronounced in the younger generations of the fluvial channel belts than in the older ones (Fig. 6 IIa). Furthermore, $D_{50 \text{ top sand}}$ values for deltaic sands become increasingly coarser in the younger generations fluvial systems (Fig. 6- IIa), notably in Zones A, B2 (Rhine channel belts) and C2 (Meuse channel belts). Some major local deviations from this downstream fining trend can be observed around X = 160 (fining dip), X = 180 (fining dip), X = 155 (coarsening spike) and X = 120 (coarsening spike) (Fig. 6 Ia). Within Zone C, (i.e. upstream of X = 160), $D_{50 \text{ top sand}}$ varies between ~240 and ~ 300 μm, and undulations are greater than downstream.

The downstream fining result for pre-deltaic deposits shows the same general trend of decreasing $D_{50 \text{ top sand}}$ from halfway the study area onwards (Fig. 6 IIIa). $D_{50 \text{ top sand}}$ values of pre-deltaic riverine deposits are only modestly larger than that of deltaic channel belt sands at the same longitudinal position. Grain sizes in the oldest generation of deltaic channel belts (Fig. 6 IIa) and the next-older '*Early Holocene channel belt deposits*' (youngest pre-deltaic unit; Fig. 6 IIIa) are mutually consistent. They show a shared downstream fining trend downstream of X = 190 km.

Delta-scale longitudinal analysis of overburden thicknesses reveals a different main break point at X = 125 (Fig. 6 IVa). The older generations of channel belts show a modest downstream increase of overburden thickness from X = 190 onwards (and sharper increase beyond X = 125). It amounts for 1–3 m in Zone C and increases to 3–5 m in Zones B and A. The younger generations of channel belt sands, however, have a fairly constant overburden thickness (Fig. 6 IVa); for the younger two channel belt generations (after 3000 yr BP) it ranges between 1 and 2 m.

5.2.2. IJssel branch (S—N downstream trends)

Longitudinal plots of $D_{50 \text{ top sand}}$ for the IJssel branch (right panels in Fig. 6) show a clear downstream fining trend for the top of sand, dropping from ~240 to ~200 μm from zone D1 to D2. Superimposed local perturbations occur, notably at Y = 465 and Y = 490 where D_{50} values spike to 300 μm. At Y = 490 these spikes seem to echo D_{50} perturbations in the *pre-deltaic* sands, which suggests local incorporation of
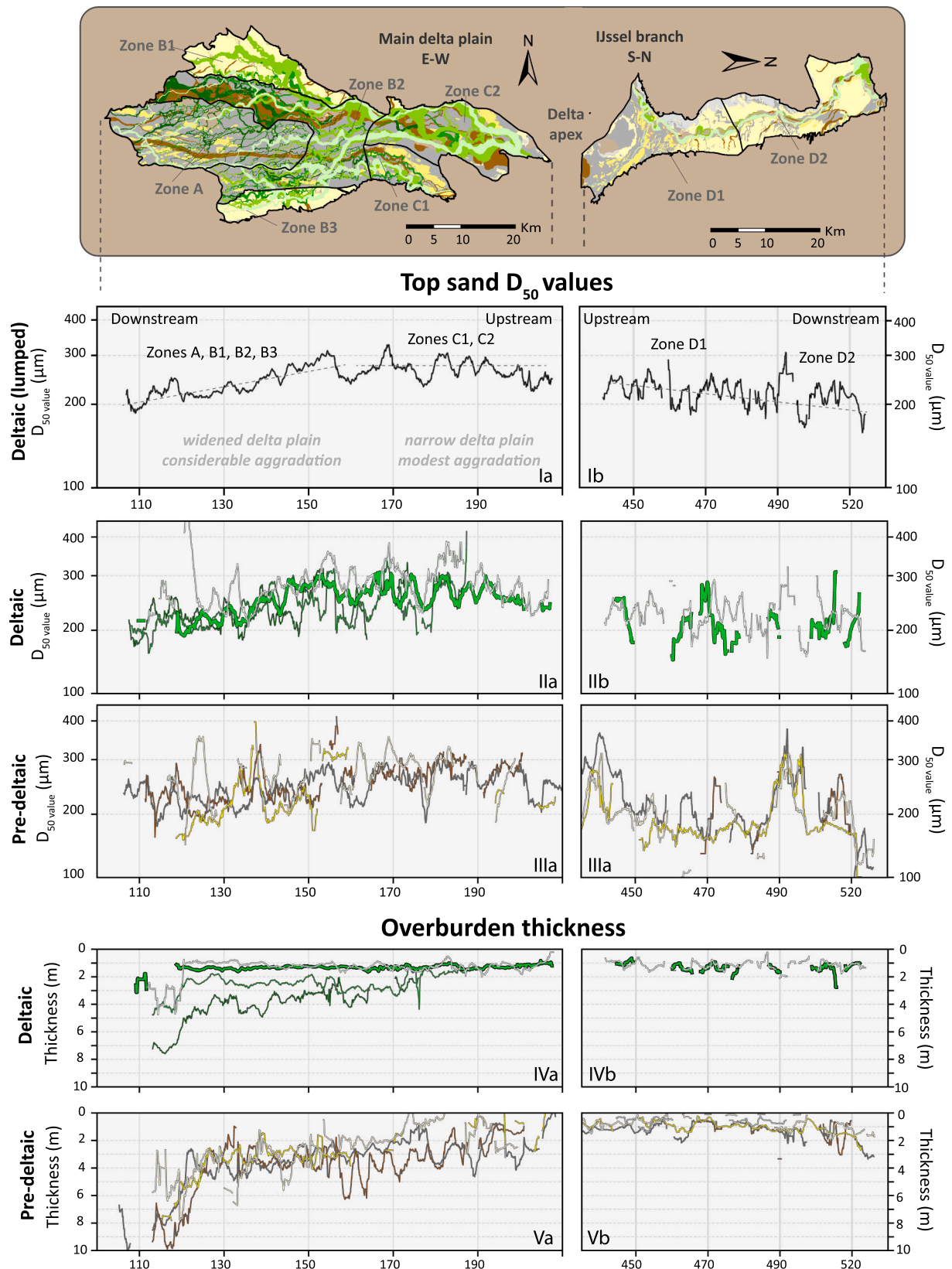
Fig. 6. Longitudinal plots of piping parameters as quantified for the Rhine-Meuse delta based on Utrecht University LLG borehole data. Left column: W-E plot, downstream direction is towards left, coordinates are easting (main delta plain): Right column: S—N plot, downstream direction is towards right, coordinates are northing (IJssel branch). Graphs show plots of D_{50} values and overburden thickness, produced using a 2 km moving-window. (I) D_{50} values, indifferent of channel belt age ('lumped'), (II) D_{50} values split by channel belt generation ({a}: $n = 1649$, {b}: $n = 4415$, {c}: $n = 8884$, {d}: $n = 3976$) (III) D_{50} values for pre-deltaic units, (IV) overburden thicknesses by channel belt generation, (V) overburden thicknesses for pre-deltaic units. Top panel maps for location references, legend as in Fig. 4.

coarser deposits ('local alluvium' in the mapping of Fig. 4). The overall fairly low $D_{50\ top\ sand}$ values (compare Zone D IJssel results in Fig. 6 IIb to those for the main delta in IIa) likely reflect regional reworking of fine-grained cover sands that occur abundantly at shallow depths (Cover Sand $D_{50\ top\ sand}$ = 185–200 μm in Zone D; Fig. 5).

Overburden thickness along the IJssel distributary is fairly constant along its entire length, with values ranging between 1 and 2 m (Fig. 5), similar to the youngest channel belts in the main delta plain (Section 5.2.1). Overburden thickness over pre-deltaic sands similarly is fairly constant. It shows modest increase from ~1 to ~3 m in the downstream most part (North of Y = 490), especially over the non-cover sand areas.

6. Discussion

Variability in lithological properties considered in piping assessments is governed by various geological controls. The ability of rivers to mix coarser sediments up in to the top of deltaic channel-belt sand bodies is the sedimentological echo of the hydraulics of river flow at the time of deposition. In addition, the composition of bed sediments can also be considered to echo the composition of the substrate that the channel cut into and reworked (sediment inheritance). The great variance observed in both the longitudinal and regional grain-size plots suggests that these two factors played an interchangeable role in explaining observed variability, which is discussed in section 6.1 below. Independent of how the regional trends are geologically explained, section 6.2 reflects on the incorporation of the geological framework with the current practice in the Netherlands and whether this approach can be utilized in other deltas around the world.

6.1. Geological controls on regional trends in lithological properties

We discuss the following geological controls on $D_{50\ top\ sand}$: (1) downstream drops in specific stream power due to downstream reduction of channel gradients (energy slope), (2) changes in substrate erodibility further affecting drops in stream power through increased channel sinuosity and (3) localized uptake and regional reworking of sediments from the pre-deltaic substrate. How these factors affected $D_{50\ top\ sand}$ in our dataset, we regard to be also be representative explanation for trends and variability in D_{70} and K_{sat} (section 2.1).

6.1.1. Hydraulic controls on grain-size variation

Specific stream power is a well-known parameter in empiric sediment entrainment and transport predictors (Van den Berg, 1995; Knighton, 1999; Makaske et al., 2011). It is determined by the product of river discharge (Q) and energy slope of its water surface (S), and calculated per unit of channel width (W). Qualitatively, it is an integrated descriptive factor, through which inherent hydraulic changes in Q, W and S in a bifurcating deltaic branch network can be summarized and used to explain the trends seen in the longitudinal $D_{50\ top\ sand}$ plots. It is used here in the latter way.

Longitudinal trend plots (Fig. 6) and further data inspection (e.g. Fig. 7) suggest downstream fining mechanisms to have affected the median grain size at the very top of deltaic channel-belt sand bodies only in the downstream part of the delta. We relate this longitudinal trend in $D_{50\ top\ sand}$ to changes in transport capacity (i.e. specific stream power). In a downstream direction, drops in the specific stream power for the typical deltaic channel belt are caused by a decrease in channel gradients reducing the energy slope (S) of the water level (e.g. Makaske et al., 2007). In the narrower upstream delta plain (i.e. Zone C), a small number of large and long-lived trunk channels maintained the network (Gouw, 2008; Stouthamer et al., 2011). The narrow, confined setting, especially during flooding events, increased the specific stream power of these systems due to concentration of the discharge (e.g. Kiss et al., 2011; Pierik, 2017). Meaning that they were able to take up and transport coarser sediments to the top of channel belt sand bodies. Further downstream where the delta plain widens (i.e. Zones B and A),

this confinement effect fades out and a downstream decrease in channel belt gradient resulted in a loss of specific stream power. This loss of specific stream power resulted in the loss of capacity of incorporating relatively coarse sediments in upper deltaic channel belt sand bodies and can explain why the downstream fining trend in Fig. 6 only appears downstream of X = 160 were the delta plain widens.

In addition to downstream changes in gradient, regional variability in substrate composition may also have resulted in regional drops in specific stream power, owing to geomorphological feedback mechanisms. Shallow-depth pre-deltaic cover sand and aeolian river dune sand are finer and more erodible than the coarser braided river deposits at larger depths (see section 6.1.2). Reduced erodibility of the local substrate can locally lead to an increased sinuosity of the river channel, which reduces the overall energy slope (S) of the water surface thus leading to a decrease in specific stream power.

In the Rhine-Meuse delta this has had particular outcome along the delta rims, most pronounced in Zone B1 (Berendsen and Stouthamer, 2000; Gouw, 2008). Here, deltaic river branches cutting into erodible cover sands at shallow depth developed relatively sinuous reaches, implying a reduced energy slope and lowered specific stream power. The combination of the finer grain sizes of cover sands leading to higher sinuosity of channels, reducing the energy slope (S) and thus the specific stream power explains the markedly lower $D_{50\ top\ sand}$ values for the younger deltaic channel belts in zone B1 compared to B2 (Fig. 5). However, over the Rhine-Meuse delta as a whole (i.e. the longitudinal plots in Figs. 6 and 7, dominated by signals from the non-rim Zones C1, B2 and A), substrate depth decreases gradually (e.g. Fig. 1B) and regional variations in erodibility align with independent drops in S, W and Q in the specific stream power. In addition, high connectivity factors throughout the entire study area (Fig. 5) imply some degree of reworking of braided pre-deltaic deposits, ruling out differences in reworking of pre-deltaic deposits as explanation for the downstream fining trend. For these reasons, we consider the specific stream power factor the main driver in explaining (1) the downstream fining trend observed in deltaic $D_{50\ top\ sand}$ values in the lower delta, and (2) the absence of such a downstream fining trend in the upper delta.

6.1.2. Sediment inheritance controls on grain-size variations

The deltaic wedge shows a considerable variation in substrate composition and associated erodibility of material that was taken up by channels intersecting these materials. Variations in substrate material may have contributed to the observed delta-scale differences in $D_{50\ top\ sand}$.

Local uptake of coarser sediments can be impacting longitudinal trends, in the $D_{50\ top\ sand}$ results between (Fig. 6- IIa-IIIa, X = 150 and 170). At X- 170, the northern trunk channel undercuts pre-deltaic flanking ice-pushed ridge relief (Fig. 1A), which is a source for coarse-grained material. Further downstream (X = 150), deltaic systems cut into relative coarse-grained braided pre-deltaic deposits (Busschers et al., 2007) that are preserved at relatively shallow depth. Sediment reworking also seems to affect $D_{50\ top\ sand}$ values on larger regional scales. Especially in regions where deltaic deposits are underlain by and encased in pre-deltaic cover sand deposits (zones B1, D1, D2), the spatial extensive opportunities of reworking of these fine-grained deposits led to the constant influx of these finer sediments into the channel belt deposits. This is clearly recognized in the results for the IJssel branch (Section 5.2.2), and can also be recognized within zone B1 at the northern rim of the main delta (Fig. 5: D_{50} values for oldest channel belt generations {a} and {b} in zone B1 are 50–70 μm finer than in zone B2 and C1).
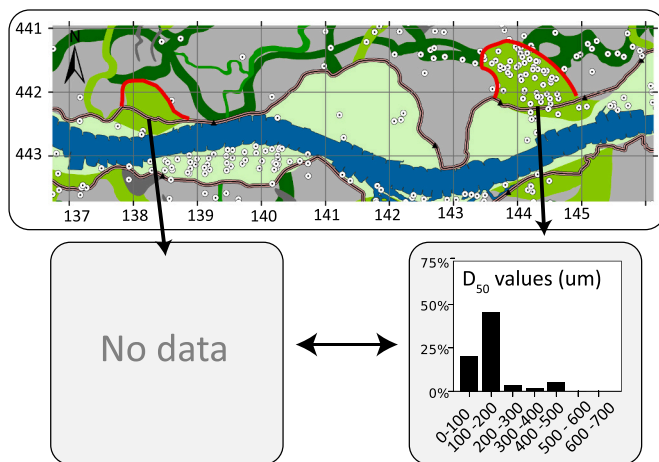
6.2. Implementation in piping assessments

We discus how implementation of geological frameworks may support local subsurface schematization and parameterizations for dike segments in delta regions in the Netherlands and elsewhere. In the

Waal river
(southern main deltaic branch last 2000 years)
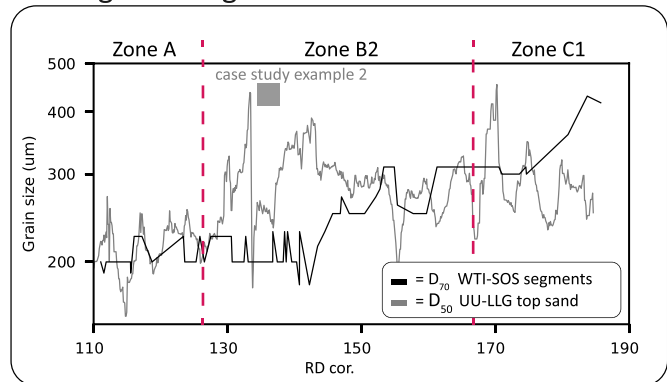
A: Longitudinal grain-size trend
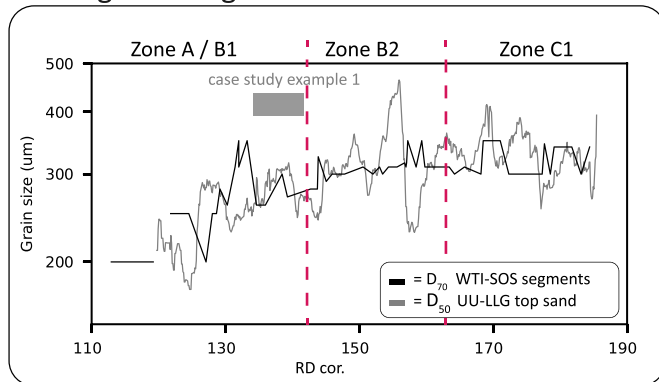
C: Case study example

Nederrijn-Lek river
(northern main deltaic branch last 2000 years)

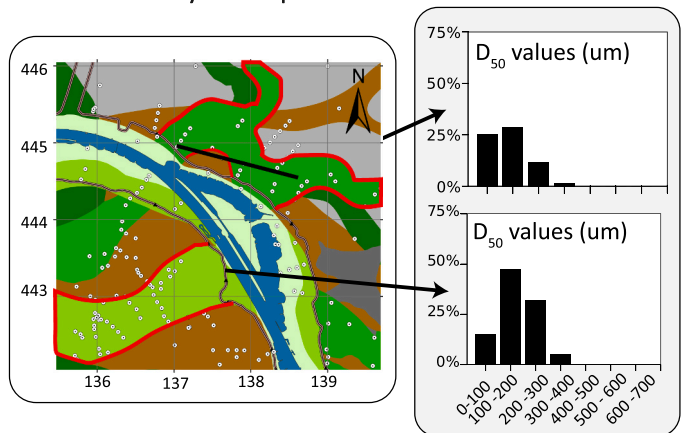### B: Longitudinal grain-size trend

D: Case study example 2

Fig. 7. Longitudinal plots of D_{50} results for individual branches Waal and Nederrijn-Lek (main delta plain; Fig. 1A). Zoomed in maps (locations in Fig. 1) and histograms of D_{50} distributions serve as examples of local application.

Rhine-Meuse delta, the large volume of available surface data (UU-LLG database) allowed for the investigation of geological casualties behind observed delta-wide trends in piping model parameters. In this case it was not just the high data coverage but the high vertical resolution of core descriptions (see Methods) that allowed to distil representative parameter values ($D_{50\ top\ sand}$) in this study. The approach was tailored to specific data availability in the Netherlands, but the principle of using regional geological considerations in subsurface schematization underneath dikes can be utilized in other deltas. For these reasons, generic aspects of the approach of this paper can be transposed to other regions throughout the world.

6.2.1. Incorporation of the geological framework with current practice in the Netherlands

In the current Dutch dike safety assessments, the WTI-SOS system provides baseline values and variance coefficients within 2 km buffer zone along dike segments (Hijma and Lam, 2015) for all subsurface piping model parameters (Fig. 2). In the directives, local parties are encouraged to adjust these default values on the basis of incorporating site-specific knowledge. The geological framework (Fig. 4) and raw and aggregated borehole database results of this paper can be used to set-up baseline values, similar to WTI-SOS, for local piping assessments. The incorporation of solely high-resolution data (UU-LLG data) puts an extra emphasis on the sandy substrate in which the backward erosion process takes place (m vs dm thick vertical schematisation). Furthermore, better

insight into the regional variance in subsurface parameters allows for the extension of incorporated data outside the typical 2 km buffer zone held within WTI-SOS. Therefore, providing an additional basis for data grouping in order to improve WTI-SOS a-priori values across comparable regions within the delta. The scheme deployed to make geogenetic distinction between e.g. channel belt generations (Fig. 4), could be useful when dividing a dike trajectory into subsections of comparable substrate at the start of the assessment of local dike segment. Vice-versa, this could make dike-safety procedural activities and WTI-SOS applications also meaningful by enlarging the insight into spatial variability in substrate characteristics below and around dike trajectories, with increasing amounts of data.

Fig. 7 illustrates the foreseen applications for two selected trajectories along the dikes of the present main Rhine branches: the rivers Waal and Nederrijn-Lek. For the entire length of the two branches, longitudinal plots show the variations in $D_{50\ top\ sand}$ based on solely high-resolution data utilized in this study and $D_{70\ top\ sand}$ default values from WTI-SOS. Both longitudinal plots are based on subsurface data within a 2 km buffer zone around the dike. The WTI-SOS $D_{70\ top\ sand}$ values reflect the upper meter of sandy deposits (compared to the upper 20 cm for our $D_{50\ top\ sand}$), and were converted from original D_{50} values by incorporating conceptual knowledge on the structure of grain size distributions (Wiersma et al., 2011). Despite underlying differences, the "D_{50}" longitudinal trends based on high resolution data and the "D_{70}" results from WTI-SOS are fairly comparable (Fig. 7). For the Waal,

longitudinal trends in $D_{50\ top\ sand}$ (this study; upper 20 cm) and $D_{70\ top\ sand}$ (WTI-SOS; upper meter) are similar: upstream of zone C1 these values are all around 300 μm, while within zone B (downstream of X = 160) a gradual downstream fining sets on (Fig. 7). For the Nederrijn-Lek upstream regional trends in $D_{50\ top\ sand}$ (upper 20 cm) respectively $D_{70\ top\ sand}$ (upper meter) also are similar, except that in WTI-SOS D_{70} marked downstream fining sets in 20-km upstream of where D_{50} in our data shows such (Fig. 7).

For two subareas along the two branches, lower panels in Fig. 7 show dike transects overlying the geogenetic mapping (as in Fig. 4) and data distribution. The example along the river Waal (Fig. 7C) represents a local scale application with limited data availability. Our geological framework identifies the dike segment to overly a channel belt of the second-youngest generation. That information allows to select a nearby cluster of borehole data points somewhat further upstream as probably representative and a fallback option to establish a D_{50} distribution to parameterize a piping calculation. The example along the river Nederrijn-Lek (Fig. 7D) illustrates the complexity of selecting representative data points where sands from several generations of channel belts occur underneath the dikes. The geogenetic scheme can be used to segregate data points, and calculate local D_{50} distributions for each channel belt generation. The mapping can also indicate in what direction to seek or how far to enlarge a search radius for representative borehole data if a minimal number is demanded. Values arrived at can be cross-checked against regionally aggregated values of the branch longitudinal plots (Fig. 7A-B), WTI-SOS defaults, and the results in Figs. 5 and 6. Furthermore, these types of analyses can be extended and densified with additional local data, to upgrade stochastic insights in order to improve the model parameterizations and routinely prepare and integrate local data of diverse background for geomechanical and flood-stage geohydrological calculations. The above procedures in practice are reliant on geogenetic mapping accuracy, and an iterative round of checking borehole data along feature boundaries and adapting boundary positions using the additional data available to dike assessment teams is recommended. This matters more in local applications exemplified in Fig. 7, than it affects the regional aggregations of Figs. 5 and 6. It is having the geogenetic scheme in the map, not the boundary accuracy, that we see as the fundamental point.

6.2.2. Generic applications of implementing geological frameworks

Also outside the Netherlands, the importance of the shallow subsurface and its geology as a major factor controlling the potential for backward erosion, has been recognized (e.g. Masannat, 1980; Kuszmaul and Glynn, 2006; Gottardi et al., 2015; Martínez et al., 2016). These studies all have a local-scale case-study character focusing on the local variability within subsurface parameters. The typical recommendation from a local study incorporating detailed geological findings, is to repeat the data-collection approach for new cases, which leads to a high demand in resources for dike improvement projects. Indeed, without a regional geological framework to slot local applications into, it is difficult to transplant locally obtained case study insights to new case studies of other dike segments. When combined with common tendencies to also gradually raise the design discharges and dike safety standards, such recommendations now have pushed piping from being a local problem to a regional problem. This can be seen as the stimulus to move to intake of subsurface information regionally (the approach in this study), and address its processing to arrive at characteristic baseline values for regions (Fig. 5).

The need for a more regional approach when assessing piping is recognized in previous studies, that advocated empirical modelling approaches to assess potential piping hazards (e.g. Glynn et al., 2012; Mazzoleni et al., 2014). Such empirical models need schematized and parameterized subsurface input. Ideally such input includes realistic regional variability, derived from geological data, but focus to actually achieve this so far has been limited.

The geogenetic mapping approach used in this study provides a rationale and data-driven starting point for realistically populating such models and assessing piping susceptibility. From a geological perspective, for the main urbanized and embanked delta plains in the world where flood safety is managed, the large scale configuration (deltaic configuration and channel network, substrate depth) as well as aggradation history (i.e. histories of base level rise and sediment delivery, overburden thickness tendencies) is generally known (e.g. Liu et al., 1992; Saucier, 1994; Amorosi et al., 2008; Carling, 2009). This understanding of the geological setting, forms the basis for the set-up of geogenetic maps (i.e. geological frameworks), allowing for transposing know forcings on trends in grainsize (section 6.1) to low data regions. This results in an a-priori regionalization of these delta plains, which in turn can be used to compare subsurface reconstructions in the vicinity of dikes thus optimizing new data acquisition campaigns.

7. Conclusion

In the Rhine-Meuse delta, variability in architectural (e.g. thickness of aquifer and overburden) and lithological characteristics ($D_{50\ top\ sand}$) of (pre-)deltaic sandy deposits are the result of sedimentary processes controlled by different geological forcings and boundary conditions. Continuous aggradation throughout the Holocene resulted in a clear relationship between channel belt age and the thickness of the overburden covering these deltaic channel-belt sand bodies, with thicknesses modestly decreasing for younger channel belt generations. Local uptake and regional reworking of sands and stream power variability all affected current $D_{50\ top\ sand}$ values of deltaic channel belt sand bodies. Likewise, where deltaic deposits are underlain by and embedded in pre-deltaic cover sand deposits, D_{50} values of deltaic deposits are regionally finer. In the upstream parts of the delta, a combination of reworking of shallow pre-deltaic deposits and relatively high specific stream power resulted in considerable variation of grain size values of the upper sand bodies, showing no longitudinal trend. The channel belt sand bodies in the downstream widened delta plain are characterized by a downstream fining trend in $D_{50\ top\ sand}$ values, due to a downstream decrease in gradients resulting in a loss in specific stream power. Local variations superimposed on this downstream fining trend are caused by local uptake of coarser Pleistocene substrate in the Holocene channel belts.

Incorporating geological context into the investigation of subsurface parameters allows for the regionalization of the study area. This regionalization allows to fine tune local subsurface reconstructions and comparison of different local sites across a regional scale. Hence, we advocate not to overlook the regional scale geological information when preparing and integrating local data of diverse background for geohydrological piping calculations at local sites. Finally, although tailored for the Netherlands, the geogenetic approach of matching relationships between genesis and geological setting on piping parameters, can be transposed to other regions throughout the world. Geogenetic mapping aids the grouping of subsurface data and thus gaining insight into the total variance of piping related subsurface parameters underneath local dike sections. In addition, a-priori regionalization of delta plain can greatly help streamline data acquisition and help to upscale schemes and insights from local case study reconstructions to a regional scale.

Declaration of Competing Interest

The authors declare that they have no known competing financial interests or personal relationships that could have appeared to influence the work reported in this paper.

Acknowledgements

Appendix. Supplementary data

Supplementary data to this article can be found online at https://doi.org/10.1016/j.enggeo.2021.106362.

References

Allen, J.R.L., 1970. A quantitative model of grain size and sedimentary structures in lateral deposits. Geol. J. 7, 129–146. https://doi.org/10.1002/gj.3350070108.

Amorosi, A., Dinelli, E., Rossi, V., Vaiani, S.C., Sacchetto, M., 2008. Late Quaternary palaeoenvironmental evolution of the Adriatic coastal plain and the onset of Po River Delta. Palaeogeogr. Palaeoclimatol. Palaeoecol. 268 (1–2), 10. https://doi.org/10.1016/j.palaeo.2008.07.009.

Apel, H., Thieken, A.H., Merz, B., Bloschl, G., 2006. A Probabilistic Modelling System for Assessing Flood risks. Nat. Hazards 38, 79–100. https://doi.org/10.1007/s11069-005-8603-7.

de Bakker, H., Schelling, J., 1966. Systeem van bodemclassificatie voor Nederland. Pudoc, Wageningen.

Beets, D.J., Van der Spek, A.J.F., 2000. The Holocene evolution of the barrier and the back-barrier basins of Belgium and the Netherlands as a function of late Weichselian morphology, relative sea-level rise and sediment supply. Neth. J. Geosci. 79 (1), 3–16. https://doi.org/10.1017/S0016774600021533.

Berendsen, H.J.A., Stouthamer, E., 2000. Late Weichselian and Holocene palaeogeographic evolution of the Rhine-Meuse delta, the Netherlands. Palaeogeogr. Palaeoclimatol. Palaeoecol. 161 (3–4), 311–335. https://doi.org/10.1016/S0031-0182(00)00073-0.

Berendsen, H.J.A., Stouthamer, E., 2001. Palaeogeographic Development of the Rhine-Meuse delta, the Netherlands. Koninklijke van Gorcum, Assen.

Berendsen, H.J.A., Hoek, W.Z., Schorn, E.A., 1995. Weichselian and Holocene River Channel changes of the Rivers Rhine and Meuse in the Central Netherlands (Land van Maas en Waal). European river activity and climate change during the Lateglacial and early Holocene. ESF Project European Paläoklimaforschung. Special issue, Frenzel, B. (Ed.). Paleoclim. Res. 14, 151–171.

Bierkens, M.F.P., 1994. Complex confining layers: A stochastic analysis of hydraulic properties at various scales. In: Netherlands Geographical Studies, 184. Utrecht University, Knag, p. 263.

Bligh, W.G., 1910. Dams, barrages and weirs on porous foundations. Eng. News 64, 708–710.

Bridle, R., Fell, R., 2013. Internal erosion of Existing Dams, Levees and Dikes, and their Foundations. Internal Erosion Processes and Engineering Assessment.

Busschers, F.S., Kasse, C., Van Balen, R.T., Vandenberghe, J., Cohen, K.M., Weerts, H.J.T., Wallinga, J., Johns, C., Cleveringa, P., Bunnik, F.P.M., 2007. Late Pleistocene evolution of the Rhine Meuse system in the southern North Sea basin: imprints of climate change, sea-level oscillation and glacio-isostasy. Quat. Sci. Rev. 26, 3216–3248. https://doi.org/10.1016/j.quascirev.2007.07.013.

Carling, P.A., 2009. The Geology of the Lower Mekong river. Biophys. Environ. Int. River Basin Aquatic Ecol. 13–28. https://doi.org/10.1016/B978-0-12-374026-7.00002-4.

Cohen, K.M., Gouw, M.J.P., Holten, J.P., 2005. Fluvio-deltaic flood basin deposits recording differential subsidence within a coastal prism (Central Rhine-Meuse delta, the Netherlands). In: Blum, M.D., Marriott, S.B., Leclair, S.F. (Eds.), Fluvial Sedimentology VII. Special Publication of the International Association of Sedimentologists, 35, pp. 295–320. https://doi.org/10.1002/9781444304350.ch17.

Cohen, K.M., Stouthamer, E., Hoek, W.Z., Berendsen, H.J.A., Kempen, H.F.J., 2009. Zand in banen - zanddieptekaarten van het Rivierengebied en het IJsseldal in de provincies Gelderland en Overijssel.

Cohen, K.M., Stouthamer, E., Pierik, H.J., Geurts, A.H., 2012. Digital Basisbestand Paleogeografie de Rijn-Maas Delta/Rhine-Meuse Delta Studies' Digital Basemap for Delta Evolution and Palaeogeography. https://doi.org/10.17026/dans-x7gsjtw.

Cohen, K.M., Dambrink, R., De Bruijn, R., Schokker, J., Hijma, M.P., 2017b. Vervaardiging van hoogtemodellen en landschapskaarten naar periode en diepte voor archeologisch gebruik in Holoceen-afgedekte delen van Nederland. Deltares Report 1210450–000-BGS-0012. DANS. https://doi.org/10.17026/dans-zck-y7wow.

Cohen, K.M., Berendsen, H.J.A., Staff LLG (Utrecht University), 2017a. Laaglandgenese boringendatabase Universiteit Utrecht. DANS. https://doi.org/10.17026/dans-zcv-knya.

De Waal, H., 2018. Basisrapport WBI 2017. Deltares Report 11202225–012–0001 pp103.

Di Baldassarre, G., Castellarin, A., Brath, A., 2010. Analysis of the effects of levee heightening on flood propagation: example of the River Po, Italy. Hydrol. Sci. J. 54 (6), 1007–1017. https://doi.org/10.1623/hysj.54.6.1007.

Dirkx, W.J., van Beek, R., Bierkens, M., 2020. The Influence of grain size distribution on the Hydraulic Gradient for Initiating Backward Erosion. Water 12 (9), 2664. https://doi.org/10.3390/w12092644.

Erkens, G., Cohen, K.M., 2009. Quantification of intra-Holocene sedimentation in the Rhine-Meuse delta: A record of variable sediment delivery. In: Erkens, G. (Ed.), Sediment Dynamics in the Rhine Catchment. Netherlands Geographical Studies, 388. KNAG/Utrecht University, pp. 117–171.

Foster, M., Fell, R., Spannagle, M., 2000. The statistics of embankment dam failures and accidents. Can. Geotech. J. 37, 1000–1024.

Frings, R.M., Hillebrand, G., Gehres, N., Banhold, K., Schriever, S., Hoffmann, T., 2019. From source to mouth: Basin-scale morphodynamics of the Rhine River. Earth Sci. Rev. 196, 1–26. https://doi.org/10.1016/j.earscirev.2019.04.002.

Glynn, E., Quinn, M., Kuszmaul, J., 2012. Predicting piping potential along Middle Mississippi River Levees. In: 6th International Conference on Scour and Erosion, Paris, pp. 1473–1480.

Gottardi, G., Marchi, M., Tonni, L., 2015. Static stability of Po river banks on a wide area. Geotechnical Engineering for Infrastructure and Development. Proc. XVI Eur. Conf. Soil Mech. Geotech. Eng. 4, 1675–1680.

Gouw, M.J.P., 2008. Alluvial architecture of the Holocene Rhine-Meuse delta (the Netherlands). Sedimentology 55, 1487–1516. https://doi.org/10.1111/j.1365-3091.2008.00954.x.

Gouw, M.J.P., Berendsen, H.J.A., 2007. Variability of channel-belt dimensions and the consequences for alluvial architecture: observations from the Holocene Rhine-Meuse delta (the Netherlands) and lower Mississippi Valley (USA). J. Sediment. Res. 77, 124–138. https://doi.org/10.2110/jsr.2007.013.

Gouw, M.J.P., Erkens, G., 2007. Architecture of the Holocene Rhine-Meuse delta (the Netherlands) – a result of changing external controls. Neth. J. Geosci. 86, 23–54. https://doi.org/10.1017/S0016774600021302.

Hesselink, A.W., Weerts, H.J.T., Berendsen, H.J.A., 2003. Alluvial architecture of the human-influenced river Rhine, the Netherlands. Sediment. Geol. 161, 229–248. https://doi.org/10.1016/S0037-0738(03)00116-7.

Hijma, M.P., Cohen, K.M., 2019. Holocene Sea-level database for the Rhine-Meuse Delta, the Netherlands: Implications for the pre-8.2 ka sea-level jump. Quat. Sci. Rev. 244, 68–86. https://doi.org/10.1016/j.quascirev.2019.05.001.

Hijma, M.P., Lam, K.S., 2015. Globale stochastische ondergrondschematisatie (WTI-SOS) voor de primaire waterkeringen. Deltares report 1209432–004-GEO-0002.

Hijma, M.P., Cohen, K.M., Hofmann, G., Van der Sperk, A.J.F., Stouthamer, E., 2009. From river valley to estuary: early to middle Holocene evolution of the lower Rhine–Meuse delta, the Netherlands. Neth. J. Geosci. 88, 13–53. https://doi.org/10.1017/S0016774600000986.

Hoek, W.Z., 1997. Palaeogeography of late Glacial Vegetations: Aspects of late Glacial and early Holocene Vegetation, Abiotic Landscape and Climate in the Netherlands. Neth. Geogr. Stud. 230, 147 pp.

Kanning, 2012. The Weakest Link: Spatial Variability in the Piping Failure Mechanism of Dikes. PhD Thesis. Delft University.

Kasse, C., 1997. Cold-climate Aeolian Sand-Sheet Formation in North-Western Europe (c. 14–12.4 ka); a Response to Permafrost Degradation and increased Aridity. Permafr. Periglac. Process. 8 (3), 295–311. https://doi.org/10.1002/(SICI)1099-1530(199709)8:3<295::AID-PPP256>3.0.CO;2-0.

Kasse, C., Vandenberge, J., Bohncke, S., 1995. Climatic change and fluvial dynamics of the Maas during the late Weichselian and early Holocene. Paläoklimaforschung 14, 123–150. https://doi.org/10.1002/(SICI)1099-1417(199705/06)12:3<209::AID-JQS306>3.0.CO;2-P.

Kiss, T., Oroszi, V.G., Sipos, G., Fiala, K., Benyhe, B., 2011. Accelerated overbank accumulation after nineteenth century river regulation works: a case study on the Maros River, Hungary. Geomorphology 135, 191–202. https://doi.org/10.1016/j.geomorph.2011.08.017.

Knighton, A.D., 1999. Downstream variation in stream power. Geomorphology 29 (3–4), 293–306. https://doi.org/10.1016/S0169-555X(99)00015-X.

Kolb, C.R., 1975. Geologic control of sand boils along Mississippi River levees. In: Coates, D.R. (Ed.), Geomorphology and Engineering: Stroudsburg. Halstead Press, Pennsylvania, pp. 99–114.

Kooi, H., Groen, J., de Vries, J.J., 1998. Problems associated with modelling sea water intrusion at large space and time scales. Ann. Geophys. 16, 443.

Kruse, G.A.M., Hijma, M.P., 2015. WTI 2017: Handleiding lokaal schematiseren met WTISOS. Deltares Report 1209432-004-GEO-0002. WTI.

Kuszmaul, J., Glynn, M., 2006. Prediction of piping erosion along Middle Mississippi River Levees - an empirical model. AGU Spring Meeting Abstracts 1, 01.

Lane, E.W., 1934. Security from under-seepage masonry dams on earth foundations. Proc. Am. Soc. Civ. Eng. 60, 926–966.

Liu, K.B., Sun, S., Jiang, A., 1992. Environmental change in the Yangtze River delta since 12,000 years B.P. Quat. Res. 38 (1), 32–45. https://doi.org/10.1016/0033-5894(92)90028-H.

Makaske, B., Berendsen, H.J.A., van Ree, M.H.M., 2007. Middle Holocene Avulsion-Belt deposits in the Central Rhine-Meuse Delta, the Netherlands. J. Sediment. Res. 77, 110–123. https://doi.org/10.2110/jsr.2007.004.

Makaske, B., Maas, G.J., Van Smeerdijk, D.G., 2008. The age and origin of the Gelderse IJssel. Netherlands J. Geosci. – Geol. Mijnbouw 87 (4), 323–337. https://doi.org/10.1017/S0016774600023386.

Makaske, B., Smith, D.G., Berendsen, H.J.A., de Boer, A.G., van Nielen-Kiezebrink, M.F., Locking, T., 2011. Hydraulic and sedimentary processes causing anastomosing morphology of the upper Columbia River, British Columbia, Canada. Geomorphology 111 (3–4), 194–205. https://doi.org/10.1016/j.geomorph.2009.04.019.

Martínez, M., Gragnano, C., Gottardi, G., Marchi, M., Tonni, L., Rosso, A., 2016. Analysis of Underseepage Phenomena of River Po Embankments. Proc. Eng. 158, 338–343. https://doi.org/10.1016/j.proeng.2016.08.452.

Masannat, Y.M., 1980. Development of piping erosion conditions in the Benson area, Arizona, U.S.a. Q. J. Eng. Geol. Hydrogeol. 13, 53–61. https://doi.org/10.1144/GSL.QJEG.1980.013.01.04.

Mazzoleni, M., Bacchi, B., Barontini, S., Di Baldassarre, G., Pilotti, M., Ranzi, R., 2014. Flooding Hazard Mapping in Floodplain areas Affected by piping Breaches in the Po River, Italy. J. Hydrol. Eng. 19 (4), 717–731. https://doi.org/10.1061/(ASCE)HE.1943-5584.0000840.

Middelkoop, H., 1997. Embanked floodplains in the Netherlands. PhD Thesis, Utrecht University.

MinIM, 2016. Achtergronden bij de normering van de primaire waterkeringen in Nederland. Hoofdrapport. Ministerie van Infrastructuur en Milieu, Den Haag, Netherlands.

NEN 5104: 1989/C1:1990 nl, 1990. Geotechniek - Classificatie van onverharde grondmonsters, 1 oktober.

Pierik, H.J., 2017. Past Human-landscape Interactions in the Netherlands. Reconstructions from Sand Belt to Coastal-delta Plain for the First Millennium AD. PhD Thesis, Utrecht University.

Pierik, H.J., Cohen, K.M., Stouthamer, E., 2016. A new GIS approach for reconstructing and mapping dynamic late Holocene coastal plain palaeogeography. Geomorphology 270, 55–70. https://doi.org/10.1016/j.geomorph.2016.05.037.

Pierik, H.J., Stouthamer, E., Schuring, T., Cohen, K.M., 2018. Human-caused avulsion in the Rhine-Meuse delta before historic embankment (the Netherlands). Geology 46 (11), 935–938. https://doi.org/10.1130/G45188.1.

Richards, K.S., Reddy, K.R., 2007. Critical appraisal of piping phenomena in earth dams. Bull. Eng. Geol. Environ. 66 (4), 381–402.

Robbins, A.B., Van Beek, V., 2015. Backward Erosion piping: a Historical Review and Discussion of influential Factors. Conference paper: ASDO Dam Safety Conference: New Orleans, LA.

Saucier, R.T., 1994. Geomorphology and Quaternary geologic history of the Lower Mississippi Valley, vol.1. US Army Engineer Waterways Experiment Station.

Schwan, J., 1986. The origin of horizontal alternating bedding in weichselian aeolian sands in Northwestern Europe. Sediment. Geol. 49 (1–2), 73–108. https://doi.org/10.1016/0037-0738(86)90016-3.

Sellmeijer, J.B., 1988. On the Mechanism of Piping Under Impervious Structures, PhD Thesis, Technical University Delft.

Sellmeijer, J.B., 2006. Numerical computation of seepage erosion below dams (piping). In: Proceedings Third International Conference on Scour and Erosion. CURNET, Gouda, The Netherlands, pp. 596–601.

Shields, A., 1936. Anwendung der Aehnlichkeitsmechanik und der Turbulenzforschung auf die Geschiebebewegung 26. PhD Thesis, Technical University Berlin.

Soil Survey Division Staff, 1993. Soil survey manual. In: USDA Agriculture Handbook 18. U.S. Government Printed Office, Washington, DC.

Stouthamer, E., Berendsen, H.J.A., 2001. Avulsion frequency, avulsion duration, and interavulsion period of Holocene channel belts in the Rhine- Meuse delta, the Netherlands. J. Sediment. Res. 71, 589–598. https://doi.org/10.1306/112100710589.

Stouthamer, E., Cohen, K.M., Gouw, M.J.P., 2011. Avulsion and its implications for fluvial-deltaic architecture: Insights from the Holocene Rhine-Meuse Delta. In: Davidson, S.K., Leleu, S., North, C.P. (Eds.), From River to Rock Record: The Preservation of Fluvial Sediments and their Subsequent Interpretation. Society for Sedimentary Geology, Special Publication, vol. 97, pp. 215–231. https://doi.org/10.2110/sepmsp.097.215.

Van Asselen, S., Cohen, K.M., Stouthamer, E., 2017. The impact of avulsion on groundwater level and peat formation in delta floodbasins during the middle-Holocene transgression in the Rhine-Meuse delta, the Netherlands. The Holocene 27, 1694–1706. https://doi.org/10.1177/0959683617702224.

Van Balen, R.T., Houtgast, R.F., Cloetingh, S.A.P.L., 2005. Neotectonics of the Netherlands: a review. Quat. Sci. Rev. 24, 439–454.

Van Beek, V.M., Knoeff, J.G., Rietdijk, J., Sellmeijer, J.B., De La Cruz, J.L., 2010. Influence of sand and scale on the piping process — experiments and multivariate analysis. Phys. Model. Geotech. 1221–1226. Delft, Netherlands. https://doi.org/10.1201/b10554-202.

Van den Berg, J.H., 1995. Prediction of Alluvial Channel Pattern of Perennial Rivers. Geomorphology 12(4), 259-279. Earth Sci. Rev. 87 (1–2), 39–60. https://doi.org/10.1016/0169-555X(95)00014-V.

Van der Meulen, M.J., Doornendal, J.C., Gunnink, J., Stafleu, J., Schokker, J., Vernes, R. W., Van Geer, F.C., Van Gessel, S.F., Van Heteren, S., Van Leeuwen, R.J.W., Bakker, M.A.J., Bogaard, P.J.F., Busschers, F.S., Griffioen, J., Gruijters, S.H.L.L., Kiden, P., Schroot, B.M., Simmelink, H.J., Van Berkel, W.O., Van der Krogt, R.A.A., Westerhoff, W.E., Van Daalen, T.M., 2013. 3D Geology in a 2D country: perspectives for geological surveying in the Netherlands. Neth. J. Geosci. 92 (4), 217–241. https://doi.org/10.1017/S0016774600000184.

VNK, 2015. De veiligheid van Nederland in kaart. Rijkswaterstaat Projectbureau VNK. Document HB 2540621, 120 p.

Weerts, H.J., 1996. Complex Confining Layers: Architecture and Hydraulic Properties of Holocene and late Weichselian Deposits in the Fluvial Rhine-Meuse Delta, the Netherlands. In: Netherlands Geographical Studies, 213. Utrecht University, KNAG /, 189 pp.

Wiersma, A., Vönhögen, L., de Klein, M., Hoogendoor, R., Gruijters, S., Maljers, D., Marges, V., 2011. Rapportage bepaling ondergrondparameters piping VNK2. Deltares Report 1203622–000-BGS-0004.

Wolff, T.F., 2002. Performance of Levee Underseepage Controls: A Critical Review. US Army Corps of Engineers, Engineering Research Center, Geotechnical and Structural Laboratory. ERDC/GSL-TR-02-19.

Ziegler, P.A., 1994. Cenozoic rift system of western and Central Europe: an overview. Geol. Mijnb. 73, 99–127.